

# Geomechanical behaviour of Opalinus Clay at multiple scales: results from Mont Terri rock laboratory (Switzerland)

Florian Amann<sup>1</sup>  · Katrin M. Wild<sup>1</sup> · Simon Loew<sup>1</sup> · Salina Yong<sup>2</sup> ·  
Reto Thoeny<sup>3</sup> · Erik Frank<sup>4</sup>

Received: 5 April 2016 / Accepted: 9 December 2016 / Published online: 16 February 2017  
© Swiss Geological Society 2017

**Abstract** The paper represents a summary about our research projects conducted between 2003 and 2015 related to the mechanical behaviour of Opalinus Clay at Mont Terri. The research summarized covers a series of laboratory and field tests that address the brittle failure behaviour of Opalinus Clay, its undrained and effective strength, the dependency of petro-physical and mechanical properties on total suction, hydro-mechanically coupled phenomena and the development of a damage zone around excavations. On the laboratory scale, even simple laboratory tests are difficult to interpret and uncertainties remain regarding the representativeness of the results. We show that suction may develop rapidly after core extraction and substantially modifies the strength, stiffness, and petro-physical properties of Opalinus Clay. Consolidated undrained tests performed on fully saturated specimens revealed a relatively small true cohesion and confirmed the strong hydro-

mechanically coupled behaviour of this material. Strong hydro-mechanically coupled processes may explain the stability of cores and tunnel excavations in the short term. Pore-pressure effects may cause effective stress states that favour stability in the short term but may cause longer-term deformations and damage as the pore-pressure dissipates. In-situ observations show that macroscopic fracturing is strongly influenced by bedding planes and faults planes. In tunnel sections where opening or shearing along bedding planes or faults planes is kinematically free, the induced fracture type is strongly dependent on the fault plane frequency and orientation. A transition from extensional macroscopic failure to shearing can be observed with increasing fault plane frequency. In zones around the excavation where bedding plane shearing/shearing along tectonic fault planes is kinematically restrained, primary extensional type fractures develop. In addition, heterogeneities such as single tectonic fault planes or fault zones substantially modify the stress redistribution and thus control zones around the excavation where new fractures may form.

---

Editorial handling: P. Bossart and A. G. Milnes.

---

This is paper #7 of the Mont Terri Special Issue of the Swiss Journal of Geosciences (see Bossart et al. 2017, Table 3 and Fig. 7).

---

✉ Florian Amann  
florian.amann@erdw.ethz.ch

<sup>1</sup> Institute of Geology, Engineering Geology, Swiss Federal Institute of Technology, Zurich, Sonneggstrasse 5, 8092 Zurich, Switzerland

<sup>2</sup> Knight Piésold Ltd., Suite 1400 - 750 West Pender, Vancouver V6C 2T8, British Columbia, Canada

<sup>3</sup> Grundwasserschutz und Entsorgung, AF-Consult Switzerland AG, Täfernstrasse 26, 5405 Baden, Switzerland

<sup>4</sup> Sektion Geologie (GEOL), Eidgenössisches Nuklear-Sicherheitsinspektorat (ENSI), Industriestrasse 19, 5200 Brugg, Switzerland

**Keywords** Clay shale · Excavation damaged zone · Undrained shear strength · Pore-pressure response · Suction · Tectonic structures · Nuclear waste disposal

## 1 Introduction

Our scientific research on the geomechanical behaviour of Opalinus Clay that we conducted in the past decade addresses fundamental behavioural aspects, associated with the short-term behaviour (i.e. the behaviour during the excavation) and the longer-term behaviour (i.e. the behaviour during the open drift phase) of the material in close

vicinity to a drift, and factors that influence the development of an excavation damaged zone (EDZ). The attempt was and is to contribute to an improved understanding of (1) the governing mechanical behaviour of Opalinus Clay, (2) the dependency of its geomechanical and petro-physical properties on the effective stress state, (3) its strength at a saturated state, (4) the short-term pore-pressure evolution during triaxial testing and tunnel excavation, (5) the processes and geological factors that control the formation of an EDZ, (6) the influence of tectonic structures at multiple scales on the EDZ, and (7) the influence of excess pore-pressure dissipation on the EDZ and tunnel deformations. The scale of investigations spans from laboratory experiments at the cm- to dm-scale to in situ experiments on the dm- to m-scale.

An overview of the experiments related to the conducted scientific research is given in Fig. 1. The work comprises a series of laboratory experiments, conducted to characterize the geomechanical properties and behaviour of intact Opalinus Clay, spanning from unconsolidated undrained (UU) shear tests (Amann et al. 2011, 2012a), unconfined compression and indirect tensile strength tests on specimens equilibrated at various relative humidity (RH) (Wild et al. 2015c), and consolidated undrained (CU) and drained (CD) triaxial tests on fully re-saturated specimens (Wild et al. 2015a). Furthermore, three in situ experiments were carried out. An overcoring experiment was used to study the evolution of a BDZ in intact rock *in situ* (Kupferschmied et al. 2015). Additionally, two mine-by experiments at the Mont Terri Rock laboratory were conducted, which focused on the interrelationships between pre-existing faults (i.e. faults planes and fault zones characterized by a high fault plane density) and excavation-induced damage at the macro and micro-scale (Yong et al. 2010, 2013; Thoeny 2014). These experiments included detailed structural and kinematic analysis using a broad range of in situ characterisation and monitoring methods, supplemented by 3D numerical modelling.

The focus of this contribution is on the characterization of the complex mechanical behaviour of Opalinus Clay, a

material at the transition between stiff soil and weak rock, by integrating the results gained in the various scientific experiments that were conducted over the past decade and have provided insights on the complexity of the geomechanical behaviour and factors that affect the development of an EDZ in the short and longer term.

## 2 Opalinus Clay at the Mont Terri Rock laboratory

Lithologically, Opalinus Clay at the Mont Terri Rock laboratory (Fig. 2) can be divided into several facies: carbonate-rich, sandy, and shaly (Thury and Bossart 1999). In this contribution, the shaly facies of Opalinus Clay at the Mont Terri Rock Laboratory is discussed. Opalinus Clay shows a pronounced micro-fabric of the clayey matrix, forming a distinct macroscopic bedding, which is related to a complex history of sedimentation, burial, physical compaction, development of diagenetic bonding, uplift, tectonic faulting, and erosion (Van Loon et al. 2004; Marschall et al. 2005). The maximum burial depth at the level of the Mont Terri Rock Laboratory was estimated to be 1350 m in the late Tertiary (Mazurek et al. 2006). The present overburden ranges from 230 to 330 m (Thury and Bossart 1999). The complex geological and tectonic history of Opalinus Clay caused a compact structure and interparticle bonding. However, no diagenetic cements that fill the pore space (such as pyrite, siderite, or calcite cement) have been found in the shaly facies (Nagra 2002). Therefore, bonding is probably more related to recrystallization of clay particles and adhesion from molecular bonds.

Opalinus Clay from the shaly facies mainly consists of clay minerals (i.e. 27–78% clay minerals composed of 15–30% illite, 5–20% illite/smectite mixed layer phases, 3–18% chlorite, and 15–22% kaolinite), and non-clay minerals (e.g. 10–27% quartz, 0.3–5% feldspar, 0.9–1.4% pyrite, and 0.8% organic matter) with a variable range of grain sizes (Mazurek 1998; Thury and Bossart 1999; Nagra 2002; Klinkenberg et al. 2009). Furthermore, carbonate bioclasts are often found (13% carbonate content). The water loss porosity of the shaly facies is in the order of 15–19% (Bossart 2008; Amann et al. 2011, 2012a; Wild et al. 2015c).

Structurally, the bedding is well-developed and the most pronounced feature at the Mont Terri Rock Laboratory. It dips towards the southeast with an angle varying between 30° at the northernmost contact to 50° at the southernmost contact (Bossart et al. 2017). Prominent tectonic features at the Mont Terri Rock Laboratory consist of three minor tectonic fault planes and a larger thrust fault (Main Fault). A detailed analysis of the tectonic setting is given in Nussbaum et al. (2011).

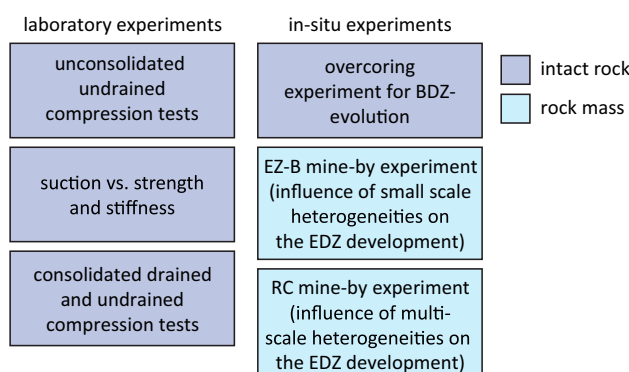


**Fig. 1** Experiments conducted at the Chair of Engineering Geology at ETH Zurich in the past decade

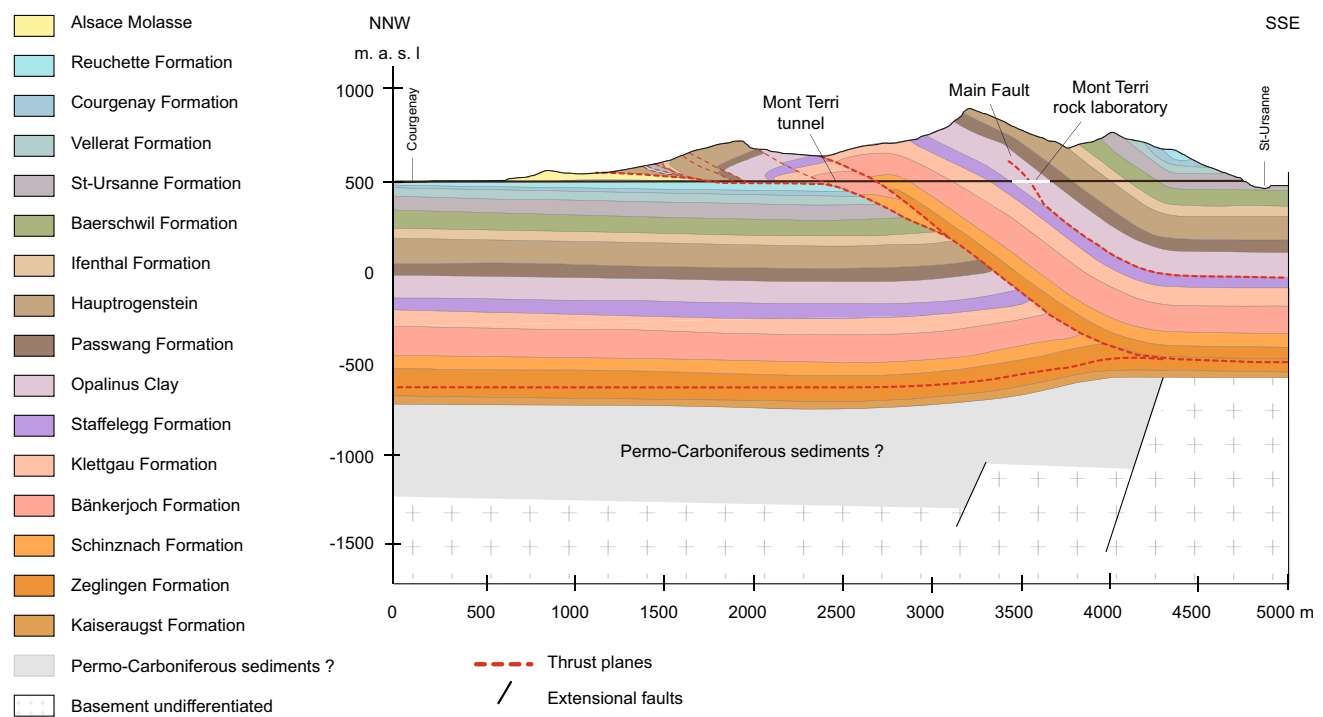


**Fig. 2** Geological cross-section of the Mont Terri anticline and location of the Mont Terri rock laboratory (Nussbaum et al. 2017, this volume)

### 3 Laboratory experiments

Three series of laboratory experiments to characterize the hydro-mechanical behaviour and properties of Opalinus Clay have been carried out in the reporting period. A first series investigated the brittle failure behaviour of Opalinus Clay under unconsolidated undrained conditions. A second series focused on the influence of suction on petro-physical and mechanical properties. In a third series of laboratory tests, we analysed the hydro-mechanical coupled behaviour of Opalinus Clay utilizing consolidated undrained and drained tests including pore-pressure measurements.

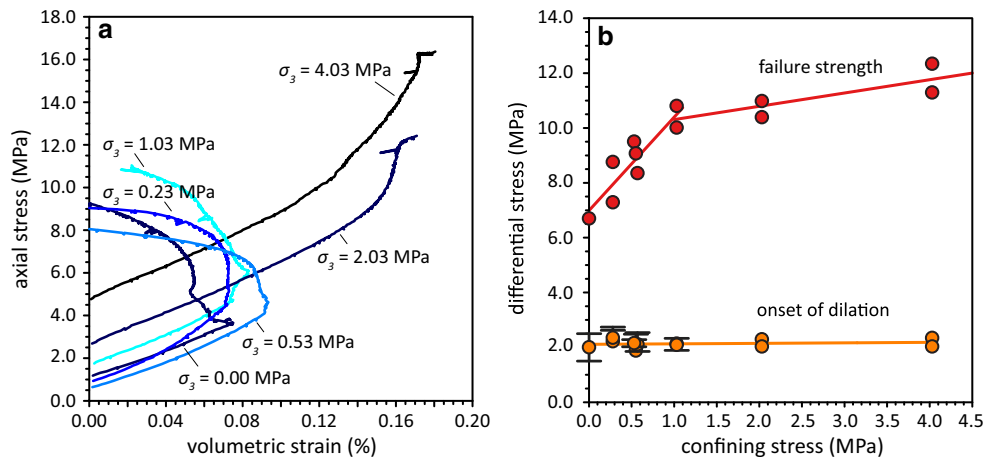
#### 3.1 The undrained shear strength of Opalinus Clay

In 2010, we performed a series of unconsolidated undrained (UU) compression tests on Opalinus Clay specimens (Amann et al. 2011, 2012a). The study focused on the brittle failure behaviour of Opalinus Clay in a confining stress range that is relevant for the near field of tunnel excavations in Opalinus Clay at the Mont Terri Rock Laboratory (i.e. 0–4 MPa). Significant efforts were made to test the specimens as close as possible to the natural water content, which required a specimen preparation procedure that allowed testing approximately 30 min after core extraction from the vacuum-evacuated foil. The specimens were loaded normal to the bedding orientation (S-specimens). Both axial and radial strains were monitored at the specimen's surface. In

addition, micro-seismic emissions were captured during the unconfined compression tests utilizing four piezoelectric transducers. More details of the testing procedure and the laboratory set-up are given in Amann et al. (2011) and (2012a).

The study revealed essential insights into the behaviour of Opalinus Clay in UU tests that demonstrate that Opalinus Clay shares similarities with both brittle rocks and stiff soils. It was shown that the onset of yielding/dilatancy is associated with the formation of micro-cracks that emanate measurable micro-seismic signals. This behaviour is typical for brittle rocks. On the other hand, Opalinus Clay deforms in a highly non-linear fashion, indicating yielding of the material long before the differential stress reaches the peak strength. The non-linearity of the stress–axial strain curve starts at the onset of dilatancy, which is unusual for brittle rocks but typical for soils, in particular clays. However, dilatancy is suppressed at increasing confining stresses. At low confining stresses the volume of the specimens at peak strength was similar to the volume of the specimens at the start of the compression test (Fig. 3a). This behaviour is typical for both brittle rock types and over-consolidated clays. Furthermore, the differential stress at the onset of dilatancy was independent of the confining stress (Fig. 3b), indicating breaking of cohesive bonds that leads to the mobilization of frictional resistance. The independency of the differential stress at the onset of micro-cracking and the mobilization of frictional resistance at the onset of dilatancy have been observed for

**Fig. 3** **a** Axial stress–volumetric strain curves before failure for different confining stresses. **b** Failure strength and onset of dilatancy in dependency of the confining stress. Adapted from Amann et al. (2012a), 27/30, copyright Springer-Verlag 2011, with permission of Springer



many brittle rock types (Martin 1997; Amann et al. 2011), but also for remoulded clays (Schmertmann and Osterberg 1960).

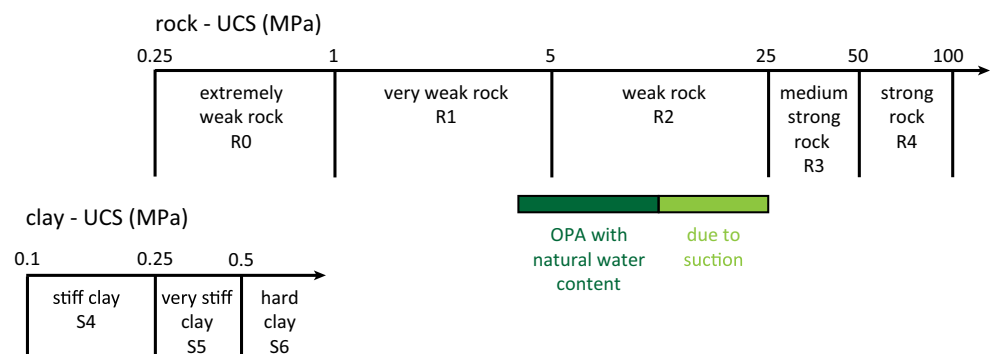
The study also revealed values of the unconfined compressive strength (*UCS*) of specimens loaded normal to bedding between 4.5 and 8.0 MPa (Amann et al. 2011). Further tests on specimens loaded parallel to bedding revealed *UCS* values between 9.0 and 11.0 MPa at natural water content (Wild et al. 2015c). Based on these values, Opalinus Clay at its natural water content can be classified as a very weak (R1) to weak (R2) rock according to ISRM classification (Fig. 4) (ISRM 1979).

A further outcome of this study was a strong non-linear failure envelope (Fig. 3b). The simplified bi-linear fit used by Amann et al. (2012a) revealed a high undrained friction angle of  $\phi = 43^\circ$  and an apparent cohesion of 2 MPa at low confinement (i.e.  $< 1$  MPa). For higher confining stresses (i.e.  $> 1$  MPa), where dilatancy of the material was suppressed, the undrained friction angle was reduced to  $\phi = 11^\circ$  and the apparent cohesion increased to 4 MPa.

Saturated clays often exhibit an undrained friction angle of zero degree. However, undrained friction angles  $> 0^\circ$  have been measured in UU tests and have been discussed in detail by Bishop and Eldin (1950), Golder and Skempton (1948) and for the specific data discussed above by Amann

et al. (2015). Bishop and Eldin (1950) proposed, based on theoretical considerations and experiments on sands, that two potential factors may account for a high undrained friction angles: (1) the specimens contain entrapped air, which increases the compressibility of the pore fluid substantially, and (2) excessive negative pore-pressure evolves under undrained shearing at low normal stresses due to the dilatant structure of the soil and causes pore-water cavitation. For the latter case, the undrained friction angle at low normal stresses is approximately the same as the effective friction angle (Bishop and Eldin 1950). At high normal stresses, cavitation does not occur and the failure envelope for typical soils indicates an undrained friction angle of  $0^\circ$  or a low undrained friction angle. The sharp transition from a high undrained friction angle to an undrained friction angle of zero depends, according to Bishop and Eldin (1950), on the undrained shearing resistance and the effective consolidation pressure. In addition, Amann et al. (2015) postulated that the concept of “ $\phi = 0^\circ$ ” applies only for soils and rocks where Skempton’s pore-pressure coefficient  $B$  is unity. For  $B < 1$ , as in the case of Opalinus Clay (Aristorenas 1992; Wild et al. 2015a), the undrained friction angle is larger than zero. Thus, for the Opalinus Clay specimens measured at low confining stresses in the series of UU tests described above, the frictional resistance

**Fig. 4** ISRM classes based on the *UCS* of the material (according to ISRM 1979). The *UCS* for Opalinus Clay at its natural water content is shown in the dark blue box. The increase in *UCS* with increasing suction is shown in the light blue box



seems to be dominated by the strong dilatant behaviour that might be associated with the microstructure of Opalinus Clay. At high confining stresses, where dilatancy is strongly suppressed, the lower undrained friction angle of  $11^\circ$  could be associated with either a Skempton's  $B$  value smaller unity or an unsaturated state of the material.

Besides the uncertainties in interpreting the UU test results, a major problem with UU tests is associated with the initial effective stress state (i.e. the effective stress state before undrained loading) of the specimen. For an isotropic rock sample taken from a rock mass characterized by an isotropic stress state, the effective stress after core extraction remains constant and the results obtained from UU tests are representative for this initial effective stress. This is, however, not the case for an anisotropic material such as Opalinus Clay taken from an anisotropic stress field such as the one observed at the Mont Terri Rock Laboratory. Thus, in the series of UU tests performed by Amann et al. (2011) and (2012a), the initial effective stress state remains unknown. Since saturation was not re-established and pore-pressure was not measured during undrained loading in their study, the interpretation and applicability of the test results in terms of the undrained shear strength remains uncertain and partly speculative.

### 3.2 The influence of suction on the strength and stiffness of Opalinus Clay

Due to the potential influence of the initial effective stress state associated with partially saturated condition, Wild et al. (2015c) performed a large series of laboratory experiments aiming at providing relationships between total suction and the Young's Modulus ( $E$ ), the Poisson's ratio ( $\nu$ ), the onset of dilatancy ( $CI$ ), the Brazilian tensile strength ( $BTS$ ), the  $UCS$ , and the P-wave velocity ( $v_p$ ). Over a period of three years, specimens were equilibrated in desiccators at different levels of relative humidity (RH) ranging between 19 and 99%. The correspondent suction pressure was calculated according to Kelvin's relationship. After specimen equilibration,  $BTS$  and  $UCS$  tests were performed immediately after removing the specimens from the desiccators. Load was applied according to the ISRM suggested methods such that failure occurred within 5–10 min for the  $UCS$  specimens and within 1–3 min for the  $BTS$  specimens (ISRM 1978, 1979). The study revealed that total suction has a major influence on both the strength and stiffness of Opalinus Clay (Fig. 5). From 0 to 57 MPa total suction,  $UCS$ ,  $CI$ ,  $BTS$  and  $E$  increases almost linearly. For suction >57 MPa, both the strength and  $E$  remain constant except for the  $BTS$  parallel to bedding, which tends to drop to smaller numbers.  $E$  increases by a factor of 3–4 between a total suction of 13 and 57 MPa (Fig. 4a),  $CI$  by a factor of 4 (Fig. 5b),  $UCS$  for tests loaded parallel to the bedding orientation by a factor of 1.5

(Fig. 5b), and the  $BTS$  parallel and normal to bedding by a factor of 2–3 (Fig. 5c).

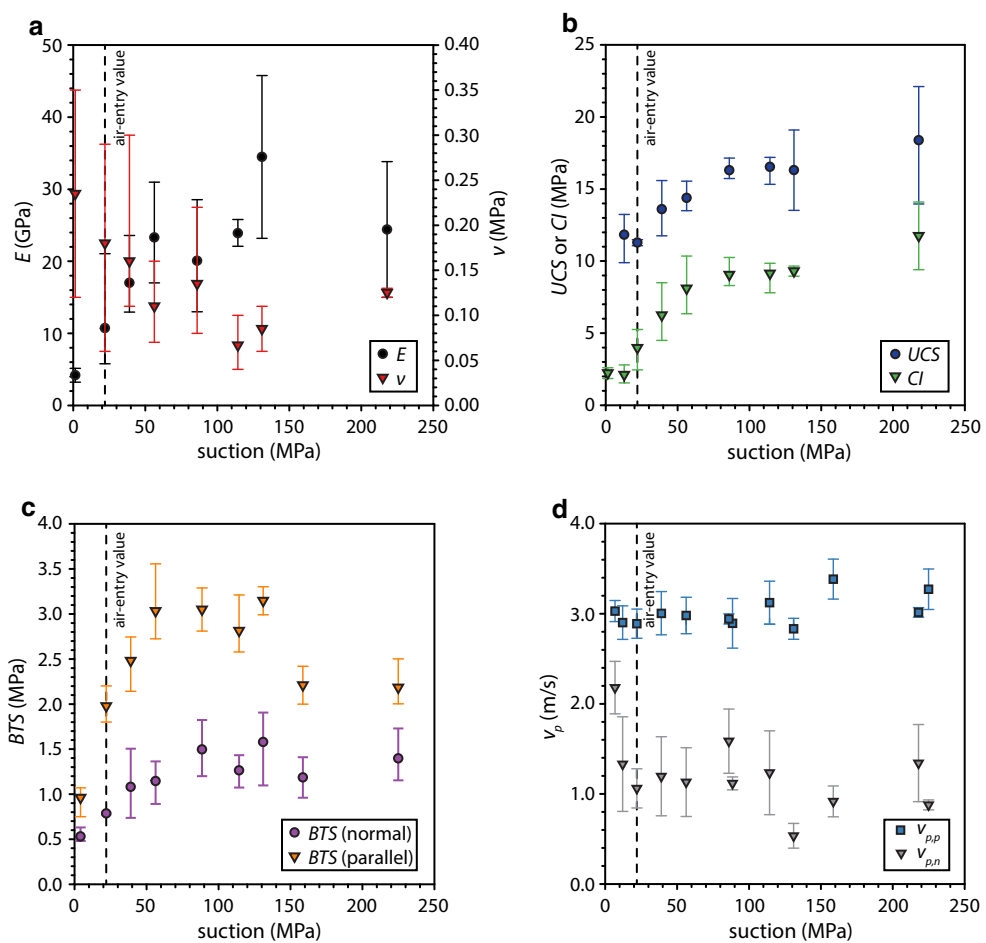
The increase in strength with decreasing water content (i.e. an increase in suction) was more pronounced for the  $BTS$  normal to bedding. Similar observations could be made by comparing the  $UCS$  values with data from tests on S-specimens (i.e. specimens loaded normal to bedding) conducted by Amann et al. (2011), Rummel and Weber (2004), and Schnier and Stührenberg (2007). The  $UCS$  for specimens loaded parallel to bedding increased from values between 9 and 11 MPa at water contents between 7.6 and 8.4% to values between 12 and 16 MPa for water contents between 4.8 and 5.0%. The  $UCS$  for specimens loaded normal to bedding showed an increase from 4–8 to 20–25 MPa for the same decrease in water content. Hence, Opalinus Clay with low water content (i.e. smaller than the natural water content due to drying) can be classified as a material somewhere between weak and medium strong rock according to the ISRM classification shown in Fig. 4.

Besides these unique relationships between total suction, water content and geomechanical properties, the study revealed that while the P-wave velocity parallel to bedding remained almost constant, the P-wave velocity normal to bedding dropped sharply upon desaturation until the air-entry value (found to be at 22 MPa suction) was reached (Fig. 5d). This drop is associated with desiccation cracks observed solely parallel to the bedding orientation. For suction larger than the air-entry value, the data suggest no further damage accumulation (i.e. the shrinkage limit is reached). Peron et al. (2009) showed experimentally for clays that the magnitude of the shrinkage limit and the air-entry value are similar. This supports the observations in our study and suggests that the majority of desiccation damage is associated with the early stage of desaturation where the suction increases from zero to approximately the air-entry value. For Opalinus Clay, the air-entry value and the shrinkage limit are reached within 30 min after core extraction from the vacuum-evacuated foil and exposure to the laboratory environment (Wild et al. 2015c). Thus, although unsaturated Opalinus Clay tends to behave more rock-like when considering the  $UCS$ , this finding shows again similarities to soil/clays, at least in the low suction regime. Despite this, this study generally suggests that in the context of an underground excavation, changes in brittle failure characteristics, stiffness and strength have to be expected when the rock is exposed to a tunnel environment characterized by a low RH.

### 3.3 Study on consolidated undrained (CU) and consolidated drained (CD) tests

As a consequence of the uncertainties associated with UU tests and the major influence of total suction on the strength

**Fig. 5** Influence of total suction on **a** the Young's modulus ( $E$ ), **b** the unconfined compressive strength ( $UCS$ ) and the onset of dilation ( $CI$ ), **c** the Brazilian tensile strength ( $BTS$ ) normal and parallel to bedding, and **d** the P-wave velocity normal ( $v_{p,n}$ ) and parallel ( $v_{p,p}$ ) to bedding. adapted from Wild et al. (2015c), 433–436, copyright Springer, Wien 2014, with permission of Springer



and stiffness of Opalinus Clay, we performed a series of CU and CD tests. The specimens were re-saturated in a long-lasting (i.e. up to several weeks) procedure that involved a flushing and a backpressure phase. Afterwards, the specimens were consolidated to different effective confinements relevant for tunnel excavations at the Mont Terri Rock Laboratory (i.e. 0.5, 0.75, 1.0, 2.0, and 4.0 MPa) and sheared by applying a standard triaxial stress path. Great attempt was taken to ensure full saturation and complete consolidation. An axial strain rate that was slow enough to either allow a reliable measurement of the pore-pressure response during undrained shearing or to avoid pore-pressure changes during drained loading was chosen. For this study we utilized both P-specimens (load is applied parallel to bedding) and S-specimens (load is applied normal to bedding).

As for the UU tests, the test results of the CU and CD tests showed similarities with both soils and rocks such as for example the dependency of the Young's modulus on the confining stress, a suppressed dilatancy with increasing confinement, and a non-linearity of the stress-strain response before peak strength. The data set revealed a relatively low cohesion in the range of 1 MPa.

Generally, a strong hydro-mechanically coupled behaviour was observed during the CU tests. In the elastic range, the pore-pressure build-up is controlled by Skempton's pore-pressure parameters  $A$  and  $B$  (Skempton 1954). Wild et al. (2015a) found that  $B$ , the ratio between the pore-pressure change and the increase in confining stress, ranges between 0.67 and 0.97 and decreases with increasing effective confinement (Fig. 6). The decrease in  $B$  is consistent with the general increase in Young's modulus and therefore related to a decrease in compressibility of the rock.

Figure 7 shows typical effective stress paths from a CU test on a P- and a S-specimen (consolidated at 2 MPa effective stress). Also plotted is the theoretical elastic effective stress path for an isotropic specimen loaded under the same conditions. A linear pore-pressure build-up is measured for all specimens up to about 0.2–4.0 MPa differential stress (dependent on the confinement). A difference in the behaviour of P- and S-specimens can be identified (Wild et al. 2015a). At low differential stress, the stress path of the P-specimen lies on the right hand side of the theoretical stress path of an isotropic poroelastic material, which indicates a lower pore-pressure build-up

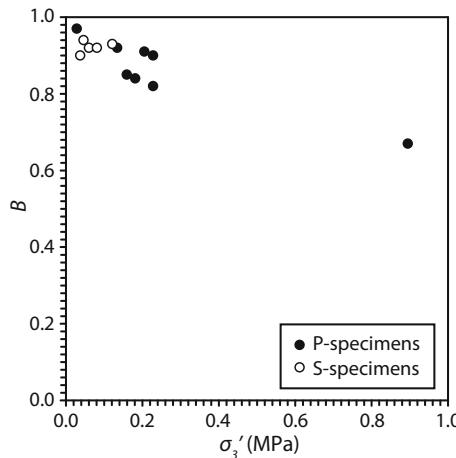


**Fig. 6** Relationship between B value and effective confinement ( $\sigma_3'$ ). Adapted from Wild et al. (2015a), San Francisco, CA, USA, 28 June to 1 July 2015, copyright 2015 ARMA, adapted with permission of American Rock Mechanics Association

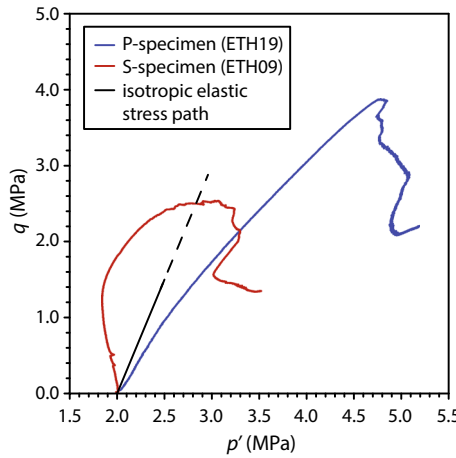


**Fig. 7** Effective stress paths for a P- and a S-specimen using a standard triaxial stress path with 2.0 MPa initial effective confinement. The black line represents the theoretical elastic effective stress path for an isotropic specimen loaded under the same conditions

compared to an isotropic specimen. For a S-specimen, the stress path lies on the left hand side of the theoretical stress path, i.e. more pore-pressure is built-up. This observation is consistent with findings of Bellwald (1990), Aristorenas (1992), and Islam and Skalle (2013). The difference in excess pore-pressure and behaviour can be related to the transverse isotropy of the clay shale (Aristorenas 1992; Bobet et al. 1999; Einstein 2000; Islam and Skalle 2013). S-specimens exhibit a higher compliance leading to a higher pore-pressure build-up compared to an isotropic material. P-specimens are stiffer than an isotropic material and therefore less excess pore-pressure is built-up.

At differential stresses of about 0.2–4.0 MPa, the specimens start to dilate and the pore-pressure increase becomes smaller with each incremental increase in

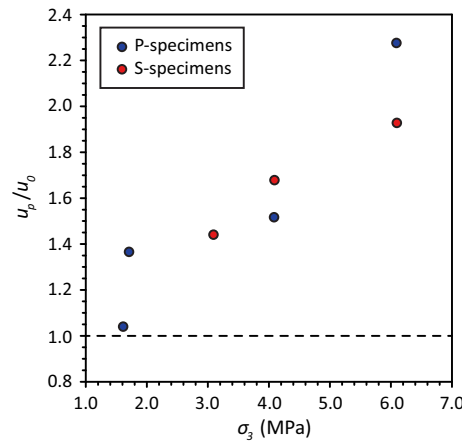


**Fig. 8** Pore-pressure at peak ( $u_p$ ) compared to the initial pore-pressure ( $u_0$ ) vs. total confinement ( $\sigma_3$ ) for P- and S-specimens. Adapted from Wild et al. (2015a), San Francisco, CA, USA, 28 June to 1 July 2015, copyright 2015 ARMA, adapted with permission of American Rock Mechanics Association

differential stress (Wild et al. 2015a). The confinement not only influences the point where dilation starts but also the amount of pore-pressure that is built-up until peak strength is reached. Whereas specimens tested at low confinement reach the peak pore-pressure before the peak strength, specimens tested at higher confining stresses show a pore-pressure increase until peak strength is reached and then drop as a consequence of the dilatancy that accompanies failure. Thus, the pore-pressure measured at peak ( $u_p$ ) for specimens tested at low confining stresses is comparable to the initial pore-pressure ( $u_0$ ) (Fig. 8). With increasing confinement, the ratio between pore-pressure at peak and initial pore-pressure increases.

Due to the low hydraulic conductivity of Opalinus Clay and the relatively high advance rate (2–20 m/day), the excavation process can be considered undrained. As a consequence, the strong hydro-mechanically coupled behaviour of Opalinus Clay can lead to significant pore-pressure changes around an underground excavation in the short-term, which influence the stability and behaviour of the rock mass. The excess pore-pressure that develops during excavation will dissipate in the longer term and may cause long-lasting deformations (e.g. swelling or consolidation) and progressive damage in the EDZ.

#### 4 In-situ experiments

In the period 2003–2015 we performed three in situ experiments (i.e., EZ-B, RC and HM-B) to examine the hydro-mechanical behaviour and EDZ evolution of Opalinus Clay on the intact rock and the rock mass scale. On the intact rock scale we investigated the time-dependent

evolution of a borehole damaged zone that develops around a borehole drilled parallel to bedding. On the rock mass scale (i.e. tunnel scale), we focused on the influence of heterogeneities such as tectonic fault planes and fault zones on stress redistribution and on the kinematic freedom for shear dislocations along tectonic fault planes.

#### 4.1 Time-dependent evolution of the damage zone around a borehole

In an attempt to better understand the evolution of the damage zone around underground excavations in intact Opalinus Clay, we performed an overcoring experiment in 2013. A pilot borehole (BHM-3) was drilled parallel to the bedding plane orientation in Gallery 08 (Kupferschmied et al. 2015). The location of the borehole is shown in Fig. 6 in Bossart et al. (2017). After core extraction, the borehole was left unsupported for 12 h and was then impregnated with a fluorescent resin (injected with a low injection pressure). After resin curing, the pilot borehole was overcored, using a 280 mm diameter bore core and the resin-impregnated section of about 1 m length was extracted. The core was cut into 30 mm thick slices that were then analysed macroscopically under UV-light and microscopically using thin sections from selected locations under a UV-light embedded microscope. The results of these analyses were used to gain detailed insight into the failure mechanism that control the short term around a circular opening in Opalinus Clay.

The BDZ was dominated by tangential shear fractures on opposing sides that intersect the pilot borehole (Fig. 9). In most of the slices, these initial bedding parallel fractures developed in only one direction (Fig. 9a). Occasionally, tangential fractures extending in the opposing directions were observed (Fig. 9b).

From the bedding parallel shear fractures tangential to the borehole wall, extensional type fractures (such as wing

cracks and horsetail splays) and secondary shear fractures emanated and propagated back toward the pilot borehole (Fig. 9). The detailed analysis of the structures revealed that the short-term BDZ is (1) dominated by shearing of bedding planes, which leads to the formation of branching fractures, is (2) localized, and is (3) only about half a pilot borehole radius deep.

Two further bedding parallel boreholes (BHG-B11 and BSE-3; for the location see Fig. 5, Bossart et al. 2017) were used to study both the evolution of BDZ structures and the extent of the BDZ with time. Borehole BHG-B11 was left unsupported for a total duration of 6 days before resin was injected and the borehole was overcored (Jaeggi et al. 2010), whereas borehole BSE-3 was left unsupported for 30 days (Badertscher et al. 2008). For the complete history of both boreholes the reader is referred to Kupferschmied et al. (2015). A comparison between the resin-impregnated BDZ structures of the different overcored boreholes delivered important insights into the development of the BDZ in relatively short durations. Within 6 days (i.e. observed in BHG-B11), the BDZ developed in both lateral and radial extent perpendicular to the bedding plane orientation and formed a chimney-like fracture network that extended at least one borehole diameter into the surrounding rock (Fig. 10a). For BSE-3, that was left unsupported for 30 days, the radial extension of the chimney like fracture network was larger than two borehole diameters (Fig. 10b). For further detailed information about the structures within the fracture network, the reader is referred to the description given in Kupferschmied et al. (2015).

The comparison between the initial and the longer-term BDZ suggests a transition from a locally damaged state characterized by shear fractures, horsetail splays, wing cracks and second order shears to a deep and delineated damage zone composed of buckled slabs in relatively short time and without further mechanical perturbation.

**Fig. 9** Sketches obtained from the macroscopic analysis of the typical BDZ-structures around a circular opening drilled parallel to the bedding plane orientation ( $S_0$ ): **a** dominating tangential fractures developed in only one direction (more often observed), **b** tangential fractures extending in opposing directions (occasionally observed). Adapted from Kupferschmied et al. (2015), 108, Copyright 2015 Elsevier Ltd., with permission from Elsevier

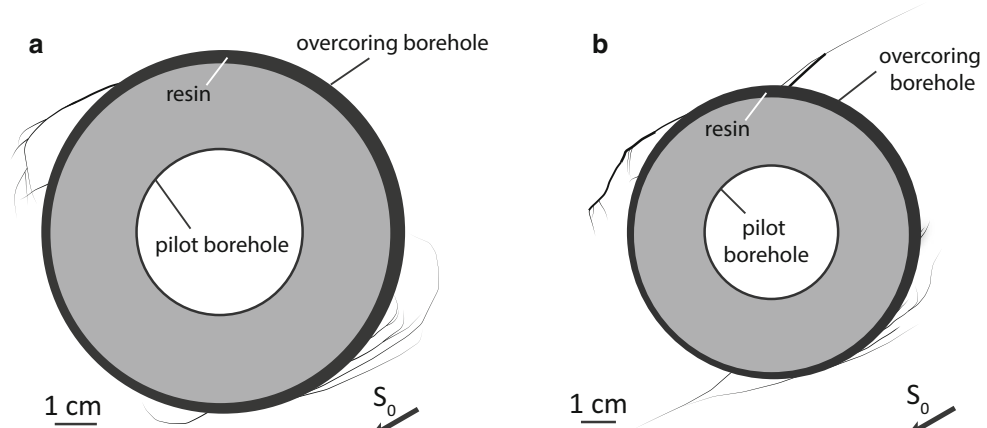
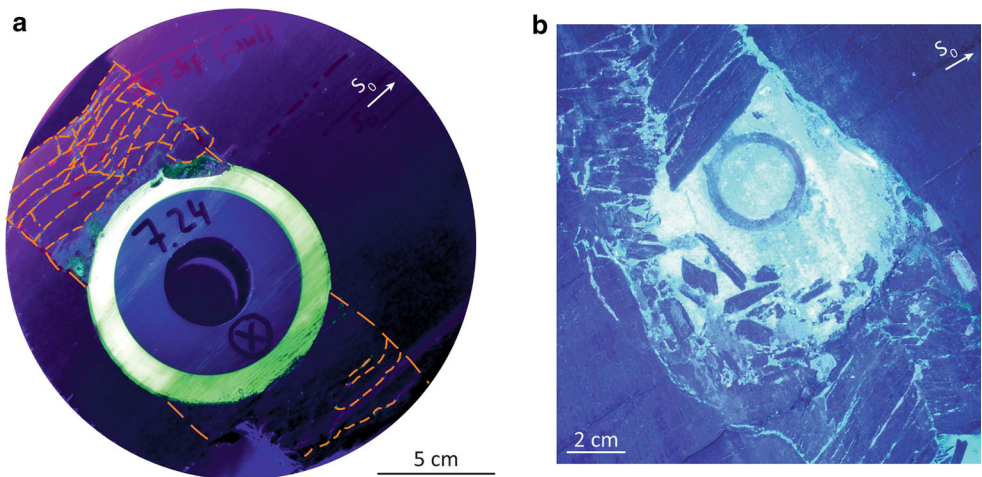


**Fig. 10** BDZ in boreholes that were left unsupported for **a** 6 days and **b** 3 weeks. Adapted from Kupferschmied et al. (2015), 111, Copyright 2015 Elsevier Ltd., with permission from Elsevier



## 4.2 EDZ evolution around Gallery 04 and the EZ-B niche

All the above studies deal with behavioural aspects of the intact Opalinus Clay. This is, however, not the case for larger underground structures like galleries at the Mont Terri Rock Laboratory where a different behaviour due to the presence of geological heterogeneities and pre-existing tectonic features has to be anticipated. Therefore, we performed two mine-by experiments aiming at gaining a better understanding of such structures on the rock mass behaviour and the development of an EDZ at multiple scales (Yong 2007; Thoeny 2014).

A first *in situ* experiment, called the EZ-B experiment, involved the excavation of a short tunnel (EZ-B Niche) with a diameter of 3.8 m and in a direction normal to the strike of bedding but oblique to the Gallery 04 axis (Fig. 5 in Bossart et al. 2017). The EZ-B Niche is located in the shaly facies, which is locally oriented on average at 147/45°. Prior to excavation, seven boreholes (BEZ-B1 to B7) were drilled for geological and geophysical characterization (BEZ-B1 to B3) as well as pore-pressure monitoring (BEZ-B4 to B7). The 1.5-m long entrance was excavated with a road header while the remaining 5 m of the niche was completed with a pneumatic hammer in six steps over a period of 12 days (Fig. 11). Additional 12 boreholes (BEZ-B8 to B19) were drilled from the niche in two vertical and one horizontal planes. An extensive program of geological, geophysical and deformation measurements was made prior to, during and after the niche excavation (Yong 2007). These consisted of: (1) geological mapping and 3D panoramic laser scanning, (2) core logging as well as optical televiewer and single-hole ultrasonic logging of boreholes, and (3) pore-pressure monitoring.

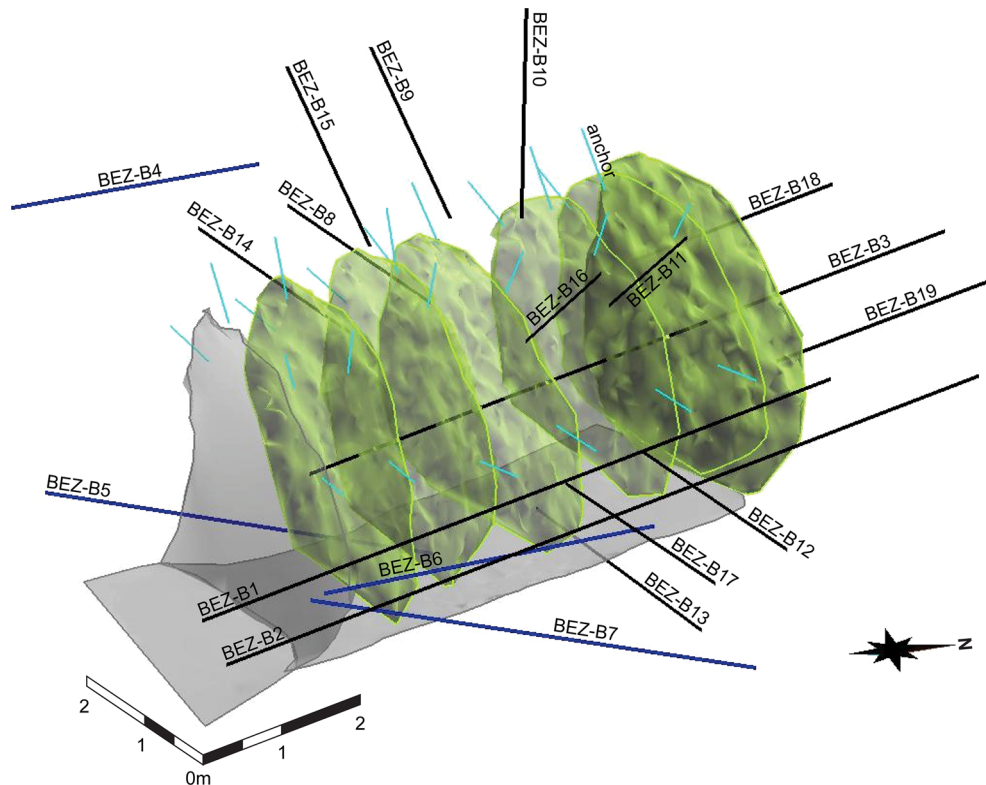
### 4.2.1 Macroscopic EDZ fracturing around Gallery 04

Detailed fracture mapping in the EZ-B niche entrance provided evidence that tectonic fault planes influenced the development of excavation-induced fracturing around Gallery 04 (Yong et al. 2010). In the west wall, the bedding-parallel fault planes were mobilized without interference from the sub-horizontal fault planes while mobilization of both sets were required to induce fracture growth parallel with the gallery wall in the east wall (Fig. 12). Numerical 2D and 3D elastic and elasto-plastic models demonstrated that if the tectonic structures (fault planes) are not kinematically restrained, their mobilization can play a key role in the development of the induced fracture network. In this case, the influence of such rock mass heterogeneity dominated over the rock matrix anisotropy of the persistently bedded Opalinus Clay that is prevalent at the Mont Terri Rock Laboratory. These results are consistent with observations made by Martin et al. (2004), Bossart et al. (2004) and Marschall et al. (2006).

### 4.2.2 Macroscopic and microscopic EDZ fracturing around the EZ-B niche

Damage around the completed EZ-B niche was investigated by fracture mapping on drillcores, televiewer images and ultrasonic logging in radial boreholes. These investigations revealed a thin inner zone of about 20 cm characterized by macroscopic fracturing and a lack of borehole instabilities (Fig. 13). This zone also coincided with the lowest P-wave amplitudes and velocities. An outer zone of increasing P-wave velocities and amplitudes was seen in the surrounding 50–70 cm. The thin macro-fractured zone was to be expected, according to a 3D numerical stress analysis that showed the rock mass most susceptible to spalling is found in the side-walls and upper western haunch, where the modelled stress

**Fig. 11** Isometric view of the various EZ-B niche faces, boreholes, and roof anchors. Reprinted from Yong et al. (2013), 302, Copyright 2013 Elsevier Ltd., with permission from Elsevier



levels only just reached a minimum to maximum principal stress ratio (spalling limit) smaller than 0.05 in the inner zone.

Rock mass damage ahead of the progressively-excavated EZ-B niche was characterized through repeat single-hole ultrasonic velocity logging and optical televiewer imaging. Furthermore, three-dimensional elastic stress analyses were conducted (Yong et al. 2013). By integrating field and numerical data, geological structures (i.e. bedding and bedding-parallel tectonic fault planes) were shown to be most influential near the entrance but diminished in role as the niche deepened (Fig. 14) and the structures became more kinematically restrained. Damage ahead of the niche face accumulated progressively as the formerly compressed volume of rock unloaded during the excavation. Low minimum to maximum principal stress ratios coincided with the lowest seismic wave velocities and amplitudes. This was corroborated in recent laboratory studies by Amann et al. (2011), who defined the brittle failure process of Opalinus Clay under undrained and low confinement conditions and demonstrated that the volumetric behaviour in the pre-rupture stage is dependent on confining stress.

#### 4.3 EDZ evolution around Gallery 08

Within the framework of the excavation of Gallery 08 at the Mont Terri Rock Laboratory, we performed a second mine-by experiment between GM 94.5 and GM 127 (RC

experiment), where Gallery 08 intersects the Main Fault of the Mont Terri Rock Laboratory (Fig. 5 in Bossart et al. 2017) and thus the rock mass exhibited a wide range of structural conditions ranging from almost massive to heavily faulted rock (Thoeny 2014). The 32.5 m long Gallery section was excavated full-face normal to the bedding plane strike in 23 steps using a road header. The bedding planes in the experimental section dip approximately 45° in the direction of the advancing tunnel face. The fracture network within the experimental section was characterized prior to and after excavation by integrating structural data from geological tunnel mapping and from 2 pre- (BRC-1 and BRC-2) and 2 post-excavation boreholes (BRC-3 and BRC-4) that were logged using an optical televiewer and geological core logging (the locations of the boreholes are given in Fig. 5 in Bossart et al. 2017). We used complementary geophysical methods including single-hole interval velocity measurements and seismic refraction tomography to quantify spatial variations in seismic velocities, rock mass properties, and the extent of the EDZ. Both displacements and deformations in the surrounding rock mass were monitored during and after completion of the excavation using borehole inclinometers, extensometers, deflectometers, high-resolution geodetic displacement monitoring, and laser scanning of excavation surfaces (Thoeny 2014).

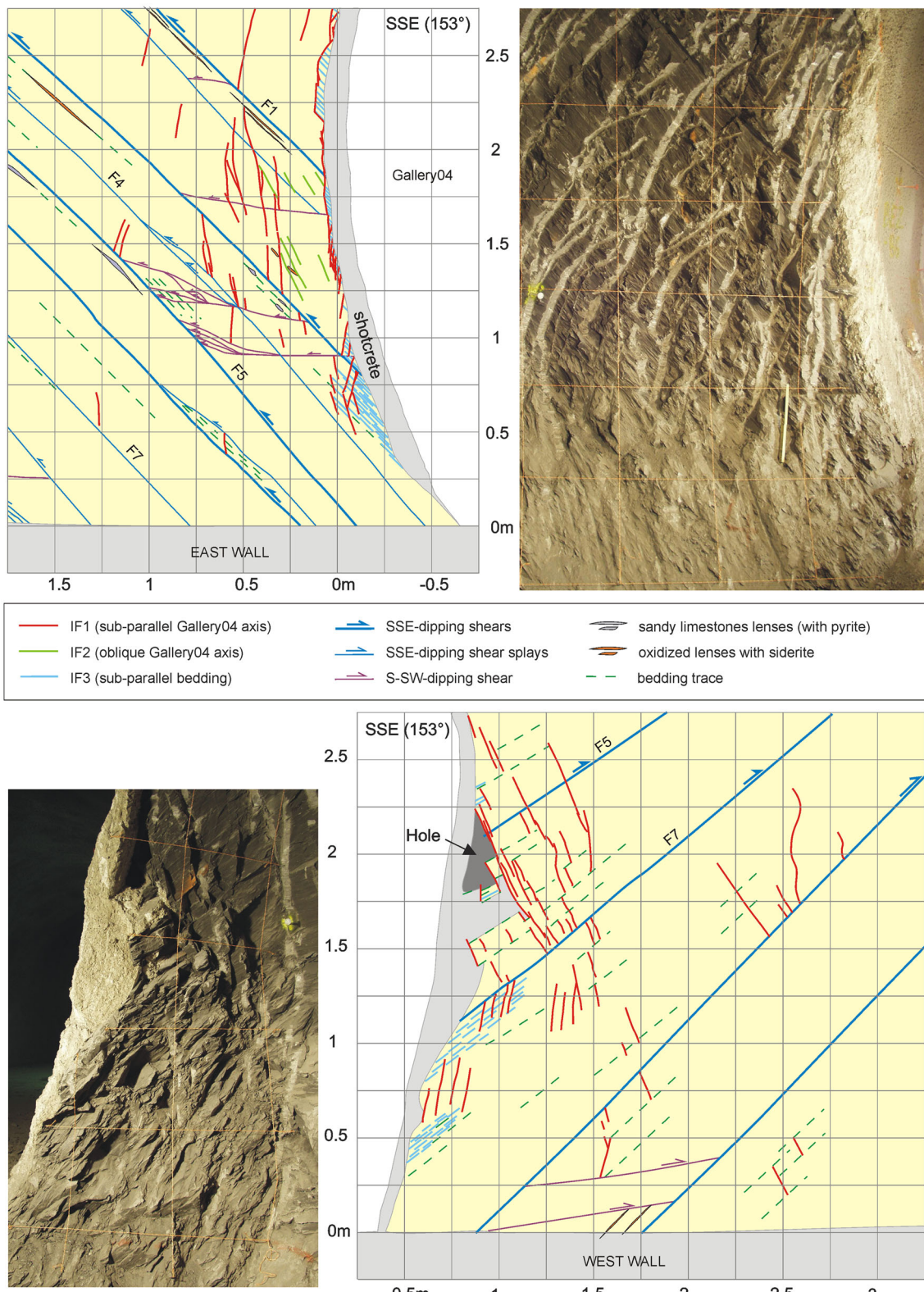


**Fig. 12** Induced fracturing mapped and photographed in the east (top) and west (bottom) walls of the EZ-B Niche entrance, parallel view with Gallery04 (maps by Christophe Nussbaum and photos by

Frank Lemy). Tectonic fault planes are labelled, ‘‘F#’’. Reprinted from Yong et al. (2010), 897, Copyright 2010 Elsevier Ltd., with permission from Elsevier

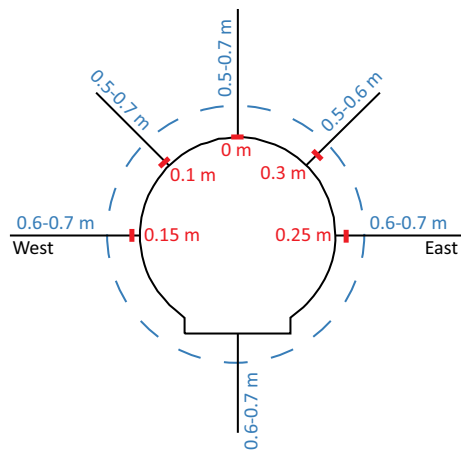


**Fig. 13** EDZ around the EZ-B niche, as determined from borehole data integration (blue). Induced macro-fracturing is shown in red. (From Yong 2007)

The integration of various geological, geophysical and deformation monitoring methods provided a unique opportunity to better understand (1) structural and kinematic relationships between natural and excavation induced fractures, (2) the spatial and temporal evolution of the excavation-induced displacement field and (3) the stress redistribution around an excavation in an anisotropic and heterogeneous clay shale formation.

#### 4.3.1 Structural and kinematic relationship between natural and excavation-induced fractures

A combination of geological and geophysical characterization techniques (i.e. geological mapping of the tunnel/niche surfaces, core logging, and seismic refraction tomography) on the tunnel and borehole scale was used to analyse the structural and kinematic influence of natural fractures on the characteristics and the spatial variation of excavation-induced damage (Thoeny 2014). The study revealed that the spatial variation in fault plane frequency along the tunnel axis has a strong influence on the rock mass strength and the deformability. This again affects the location and the radial extent of the induced damage at both borehole and tunnel scale. Based on the observations, a conceptual model of the EDZ around the mine-by section was established (Fig. 15). A strongly damaged inner zone with a radial extent of 0.5–1.5 m was observed which is unaffected by variations in fault plane density along the tunnel axis. Furthermore, a less damaged outer zone which changed in radial extent depending on the fault plane density was identified. Within the main fault, the radial extent of this outer zone reaches up to a distance of 4 m, whereas between fault zones the outer zone extends to

2–3 m. The EDZ around the RC section consists of reactivated fault planes and seven different types of induced fractures (IF) (Fig. 16):

- (IF 1) extensional fractures parallel to the sidewalls
- (IF 2) extensional fractures oblique to the tunnel axis at the sidewalls
- (IF 3) sub-horizontal extensional fractures parallel to the tunnel invert
- (IF 4) extensional and/or shear fractures along bedding planes at the tunnel invert
- (IF 5) extensional fractures perpendicular to sheared bedding or reactivated fault planes at the tunnel invert
- (IF 6) shear fractures along bedding planes at the tunnel face
- (IF 7) extensional fractures sub-perpendicular to sheared bedding planes or reactivated fault planes at the tunnel face.

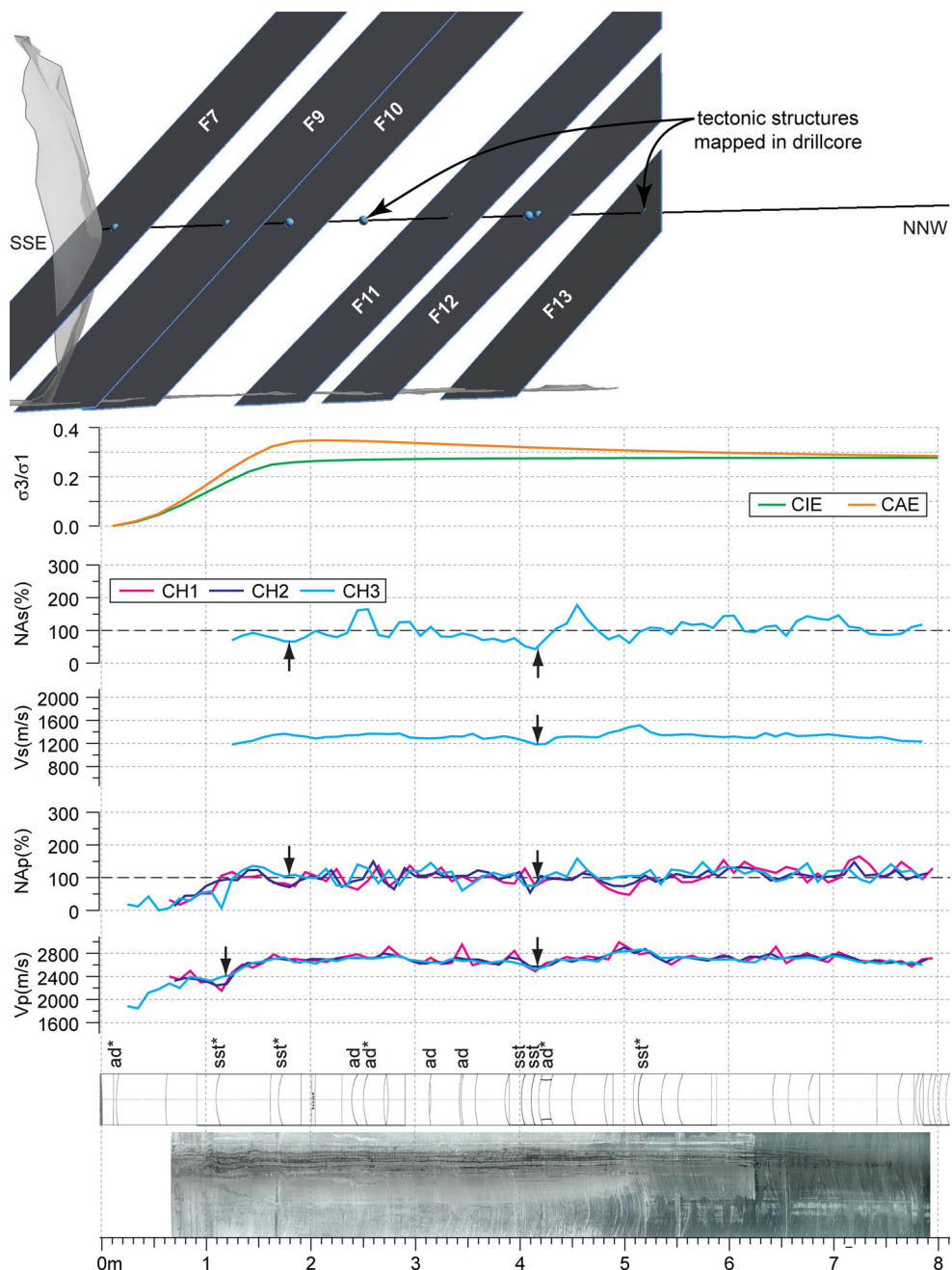
The failure mechanism, orientation, and frequency of these induced fractures are strongly influenced by the occurrence and characteristics of multi-scale tectonic fault planes. Extensional fracturing (IF1–IF2) dominated at the sidewalls where fault plane reactivation and bedding shear are constrained due to high normal stresses. Depending on the fault plane frequency, different IF were observed at the tunnel invert or tunnel face where fault plane reactivation and bedding plane shear are kinematically free. In sections where the rock mass is sparsely faulted ( $0\text{--}1$  fault/ $\text{m}^2$ ), extensional brittle failure and shearing along bedding planes (IF3–IF4 at invert, IF6 at tunnel face) were observed. In sections where the rock mass shows a higher fault plane frequency ( $1\text{--}3$  faults/ $\text{m}^2$ ), the EDZ is mainly composed of IF5 (invert) or IF7 (face) fractures. In sections with even higher fault plane density ( $>4$  faults/ $\text{m}^2$ ), reactivation of densely spaced fault planes becomes more evident and macroscopic EDZ fractures described above diminish, which indicates a transition from extensional macroscopic failure to shearing.

#### 4.3.2 Spatial and temporal evolution of the excavation-induced displacement field

The influence of pre-existing fault planes and fault zones on excavation induced displacements and deformation in the short and longer term was analysed on the fracture and tunnel scale (Thoeny 2014). On the borehole scale, vertical, radial, and longitudinal displacements were monitored using a TRIVEC, a deflectometer, and two extensometers. The data was recorded during the excavation phase as well as in the longer term (up to 2.5 years after installation). Additionally, laser scanning monitoring of the tunnel surface was used. The analysis of the data revealed that the overall rock mass response of faulted Opalinus Clay is mainly controlled by the rock anisotropy. Heaving

**Fig. 14** BEZ-B3 borehole data with asterisks indicating drillcore structures mapped closest to projected intersections of bedding-parallel shears, represented by arrows.

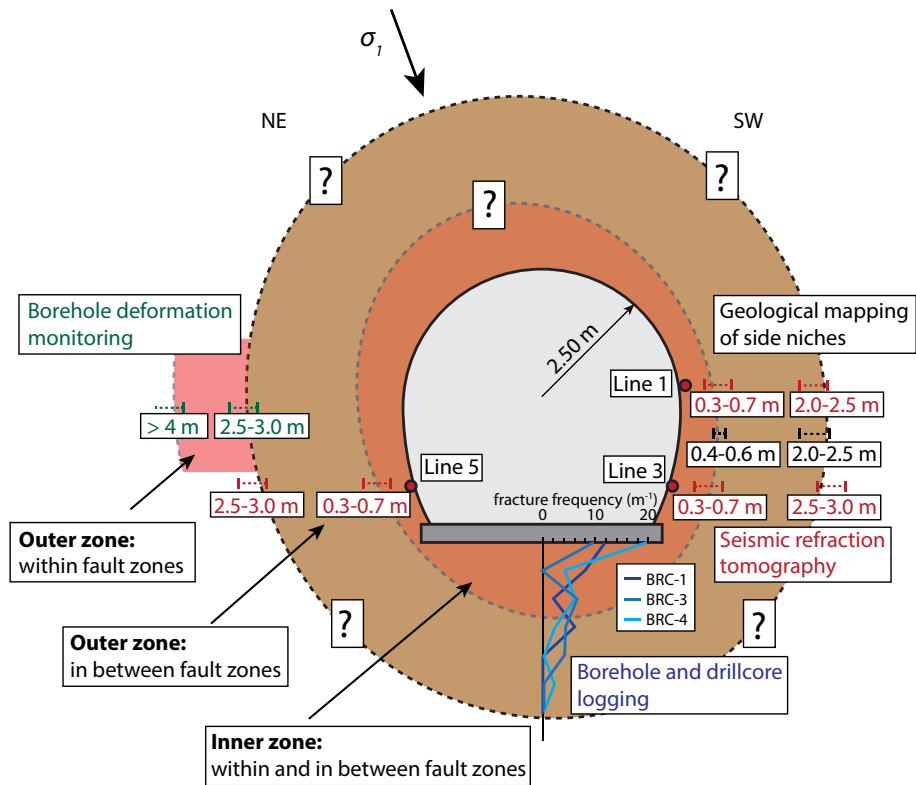
Reprinted from Yong et al. (2013), 306, Copyright 2013 Elsevier Ltd., with permission from Elsevier



observed at the lower sidewalls and below the tunnel invert as well as settlements at the tunnel crown and upper sidewalls suggest that the preferred displacement orientation is sub-perpendicular to the bedding. Furthermore, the displacement field and magnitude at the tunnel face, crown and invert is influenced by individual pre-existing fault planes. At the sidewalls, the orientation of the fault planes with respect to the tunnel is kinematically rather unfavourable for shearing along them and the response is dominated by extensional fracturing through the intact rock matrix. This results in the formation of slab-like structures behind the tunnel face associated with large displacements.

Continuous borehole monitoring by deflectometer and extensometers showed that longer-term rock mass deformations parallel to the rock anisotropy are substantially smaller than deformations occurring during the excavation phase. This is in contrast to the measurements of the inclinometer which indicate significantly larger displacements in the longer term compared to the short term, especially in the vertical direction, oblique to the bedding. Parallel to bedding, the short-term rock mass deformations are controlled by differential deformations along fault planes. The longer-term response, on the other hand, is not significantly affected by these large-scale heterogeneities

**Fig. 15** Conceptual model of the excavation damaged zone based on borehole information, geological mapping, seismic tomography, borehole and drillcore logging and deformation measurements in BRC-2 (the location of the borehole is given in Fig. 5 of Bossart et al. 2017, this volume) (Figure modified from Thoeny 2014)



but rather related (especially in the tunnel invert) to the extent of the initial (short-term) EDZ.

#### 4.3.3 Stress redistribution

Site-specific three-dimensional numerical models were used to investigate the influence of rock mass characteristics (i.e. large-scale deformability and strength heterogeneities related to multi-scale fault zones) on the excavation-induced stress redistribution during tunnel excavation and the associated short-term rock mass response (displacements) in the tunnel near-field (Thoeny 2014). Both the elastic and plastic response around the mine-by section was simulated using the commercial three-dimensional continuum code FLAC3D (Itasca 2009). The total stress approach was used and the short-term behaviour during excavation was assumed to be undrained. First, an elastic analysis with an isotropic and transversal isotropic model was conducted to identify the influence of the rock anisotropy (related to the bedding planes) and the rock mass heterogeneity (related to fault zones) on the stress and displacements. Afterwards, an elasto-plastic model was used to quantify the effect of the stress redistribution on the displacements and the extent of the EDZ. Further details to the models are given in Thoeny (2014).

The elastic models revealed that substantial stress concentration in the rock mass adjacent to fault zones can be related to large-scale heterogeneities in deformability (i.e.

caused by spatial variations in fault plane frequency; the contrasts in deformability were derived from single-hole interval velocity measurements which suggest various zones of similar P-wave velocities; it was assumed that the computed contrasts in the dynamic Young's modulus are the same for the static Young's modulus). The magnitude and extent of these stress concentrations are proportionally related to the stiffness contrast between fault zones and the intact rock mass. The study further showed that isotropic heterogeneous models with an average Young's modulus used for the intact rock mass can sufficiently represent the changes in stress magnitudes in a transversally isotropic rock mass, at least for the orientation of the tunnel with respect to the bedding plane orientation encountered in the RC experiment. Furthermore, the constitutive model (i.e. isotropic/transversely isotropic) only influences the orientation of the displacement vector but not its magnitude. Also the stress path is unaffected. Stress path analyses allowed to identify kinematic failure modes occurring during tunnel excavation. Generally, shearing along fault and bedding planes dominate at the face, invert and crown. This findings are consistent with Martin et al. (2004) and Nussbaum et al. (2011). However, differences in initiation of shearing and the associated type of faulting were observed. At the face, the reactivation of fault and bedding planes is initiated ahead of the face (2–3 m for faults, 0.5–1 m for bedding planes) and is consistently associated with normal faulting. At the invert/crown, the initiation of

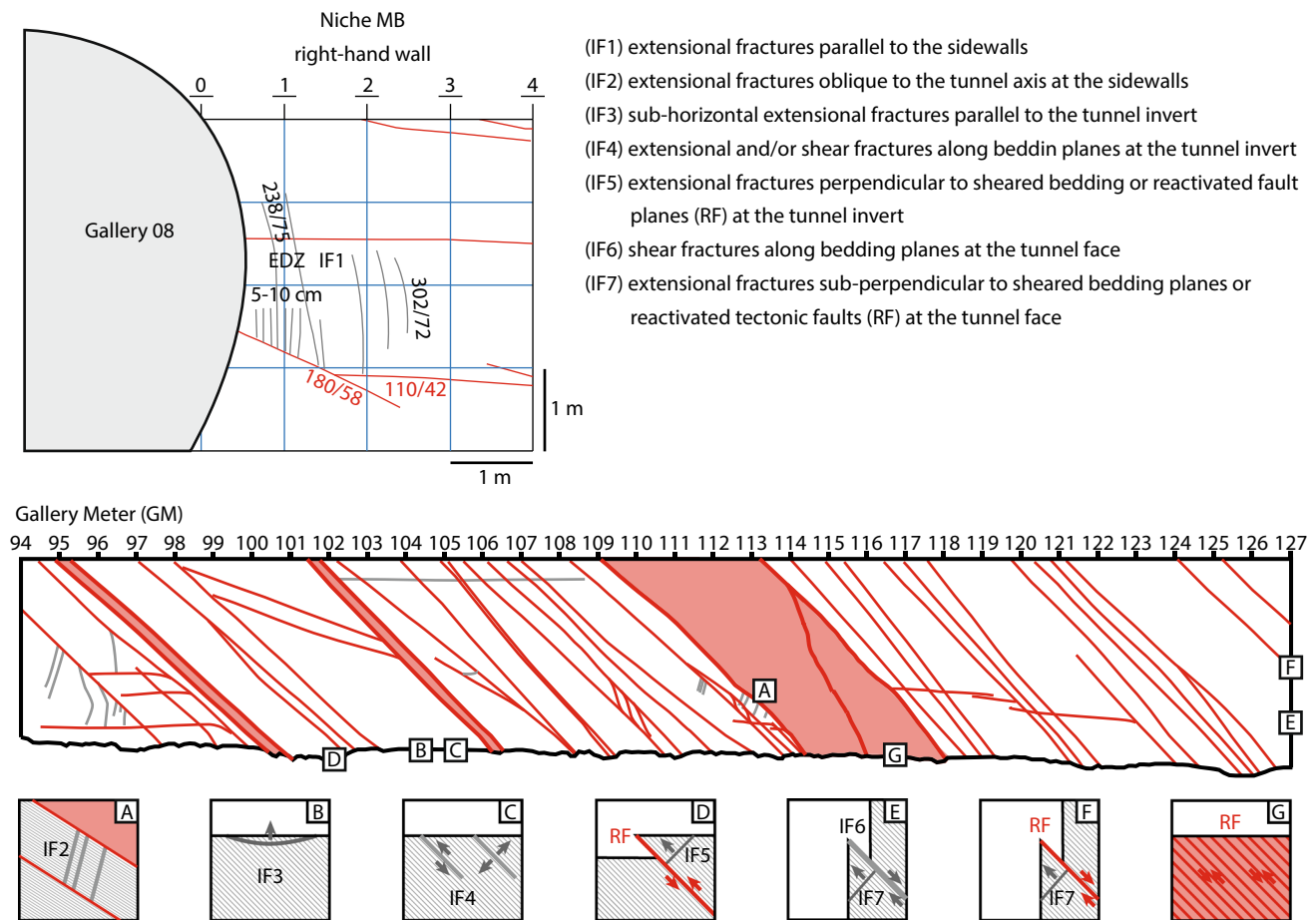


**Fig. 16** Conceptual model that illustrates the structural and kinematic relationship between pre-existing tectonic fault planes and excavation induced fractures around the RC-mine-by section. (Figure modified from Thoeny 2014)

fault and bedding plane shear takes place behind the face and is associated with reverse faulting. Furthermore, extensional fracturing was identified as the primary failure mechanism at the sidewalls. Extensional fractures may also form sub-parallel to the tunnel face in the vicinity of fault zones where stresses are significantly augmented. All these findings are consistent with field observations.

The elasto-plastic models showed that variations in rock mass strength and deformability along the tunnel axis have a significant influence on the extent of the EDZ. The modelled radial extent and its variation are consistent with the conceptual model of the EDZ described above (Fig. 15). Furthermore, the spatial and temporal evolution of the displacement field as well as the measurable displacement magnitudes of the models are generally in good agreement with the measured values. The magnitudes are only not captured in zones where structural controlled instabilities (slab-like features) or major side-wall slabs associated with dilatant behaviour develop. Nevertheless, these zones correspond in extent and location to the maximum modelled plastic shear strain.

## 5 Discussion

### 5.1 The importance of the effective stress state on the stability of Opalinus Clay excavations

The relatively low cohesion tested in CU and CD test on back-saturated Opalinus Clay specimens would suggest that tunnel deformations at the Mont Terri Rock Laboratory may be large. For the stress state at the Mont Terri Rock Laboratory, significant squeezing of the rock mass into the tunnel excavation could be anticipated. However, excavation sidewall and faces are, except for instabilities which are associated with pre-existing tectonic structures or large side-wall slabs, stable or show only small to moderate short-term deformations [i.e. 1–2 cm in case of excavations normal to the bedding orientation (Thoeny 2014) and 2–4 cm parallel to the bedding orientation (Martin et al. 2011)]. The short-term stability is likely associated with the effective stress state that evolves as a consequence of tunnelling stress path, which may cause a short-term apparent cohesive strength component. This is

illustrated in the following, based on experience gained from the above experimental studies, theoretical considerations and conceptual numerical modelling.

### 5.1.1 Apparent cohesion in a bore core

The effective stress state in a bore core extracted at the Mont Terri Rock Laboratory can be illustrated with a simple model of a bore core that is unloaded from its in situ state of stress. At the Mont Terri Rock Laboratory, the mean total stress  $\sigma_m$  is 4.5 MPa according to Corkum and Martin (2007), the in situ pore-pressure  $P$  is approximately 2.0 MPa and thus the effective mean stress  $\sigma'_m$  is 2.5 MPa. Assuming isotropic elastic conditions, the pore-pressure drop can theoretically be estimated using the following expression,  $\Delta P = B\Delta\sigma_m$ , where  $B$  is Skempton's pore-pressure coefficient (Skempton 1954). Assuming  $B$  is at unity, the pore-pressure in the bore core is -2.5 MPa after core extraction although the effective stress remains constant. Thus, a substantial apparent cohesive strength component is to be anticipated which stabilizes the core until pore-pressures that develop in the short term dissipate. For the anisotropic stress state at the Mont Terri Rock Laboratory and for the assumption of a transversal isotropic material behaviour, the effective stress in the bore core depends significantly on the drilling orientation with respect to the principal stress components. We used a simplified numerical model to estimate the negative pore-pressure in a bore core with different orientations of the plane of anisotropy in respect to the stress state at the Mont Terri Rock Laboratory. The model consists of a single cell in FLAC3D (Itasca 2009) which is unloaded to atmospheric conditions from an in situ state of stress similar to the state of stress in the Mont Terri Rock Laboratory. The model geometry is shown in Fig. 17.

We used an elastic, transversal isotropic model that does not account for any plastic deformations. We analysed various orientation of the plane of anisotropy and we

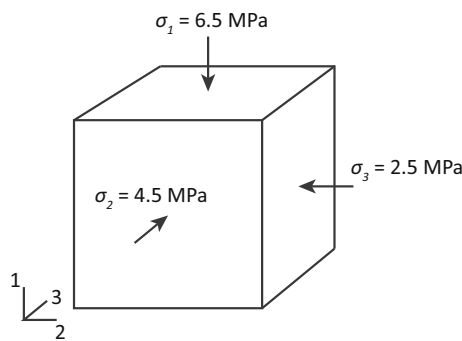


**Fig. 17** Model geometry of the conceptual three-dimensional model conducted to estimate the negative pore-pressure in a bore core with different orientations of the plane of anisotropy

assumed different ratios between  $E_1$  and  $E_3$  (i.e. the Young's moduli normal and perpendicular to the bedding plane orientation) ranging between 0.5 and 3. Note that this model does not intent to capture the complexity associated with drilling and core extraction as for example described in detail in Pei (2003). The results are illustrated in Fig. 18 which shows the modelled pore-pressure in a sample that developed upon unloading for the assumption that the plane of anisotropy is rotated about axis 2 (Fig. 18a), axis 1 (Fig. 18b) and an axis that is 45° inclined from axis 1 (Fig. 18c). Fluid pressure between -0.5 and -3.5 MPa can be anticipated and suggest that the short-term stability of bore cores is primarily due to negative fluid pressures that evolve during bore core unloading and an associated apparent cohesive strength component.

### 5.1.2 Apparent cohesion around a borehole

Our overcoring experiment showed that the short-term damage zone that evolves around a borehole drilled parallel to the bedding directions is very localized and dominated by shearing along bedding planes that are tangential to the borehole wall and branching fractures. The extent of the initial BDZ (i.e. after 12 h) was in the order of 0.25 times the radius of the pilot borehole. After 6 days, the BDZ depth was about two diameters of the pilot borehole and twofold wider than the initial BDZ. Within only 30 days, an unsupported borehole collapsed and the BDZ increased rapidly in extend and depth. Kupferschmied et al. (2015) concluded that the limited extent of the BDZ in the short term is associated with an effective stress state that favours stability of the borehole and evolves as a consequence of unloading and dilatant failure immediately during drilling (i.e. negative excess pore-pressures develop that increase the effective stress).

The rapid development of the BDZ within 30 days could be related to different processes such as dissipation of excess pore-pressure, creep, and processes related to seasonal variations in climatic conditions (RH or temperature). However, the observations revealed that the evolution from an initial state to a longer-term state occurs relatively fast. This suggests that the evolution of the BDZ is likely controlled by pore-pressure dissipation, which destabilizes the borehole, rather than by creep or climatic variations. Destabilization is associated with a propagation of initial tangential shear fractures and the formation of further bedding parallel shear fractures deeper in the rock mass. These bedding parallel shears form slabs that tend to buckle into the borehole until collapse occurs. The hypothesis that excess pore-pressure dissipation dominates the long-term behaviour of underground excavations is in agreement with the conclusions from Martin et al. (2004), numerical findings performed by Amann et al. (2012b),

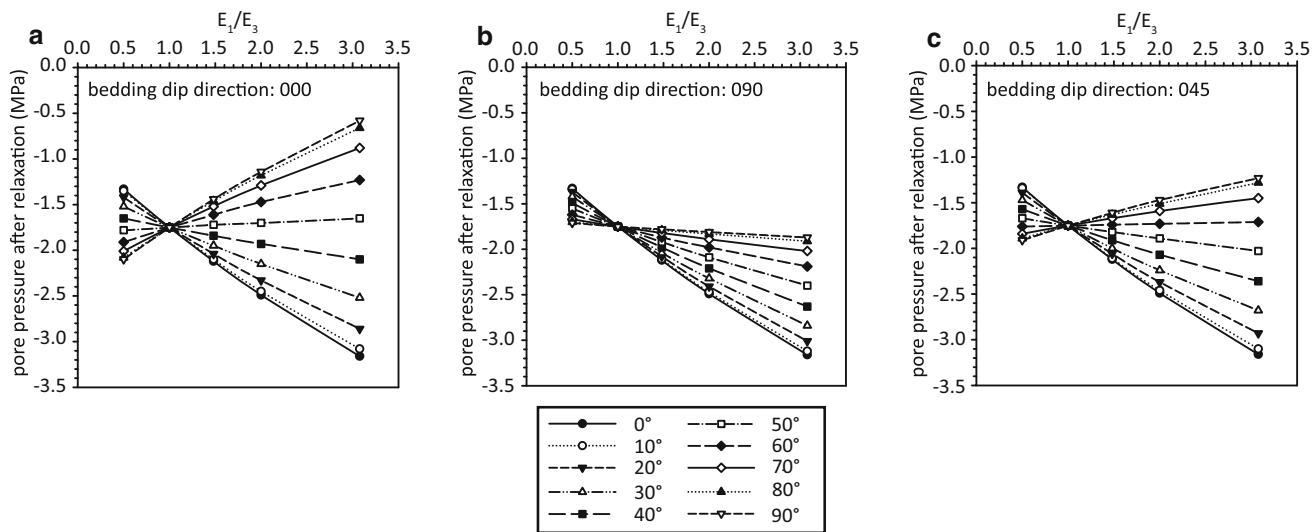


**Fig. 18** Theoretical pore-pressure after relaxation of a bore core from an in situ state of stress equivalent to the state of stress at the Mont Terri Rock Laboratory. Dip direction is measured positive clockwise

in the horizontal plane from *axis 3* (Fig. 16), which is zero degrees in azimuth. Dip is measured positive down from the horizontal plane (*plane 2–3*)

experimental data reported by Neerdael et al. (1999), and theoretical considerations reported by Anagnostou (2009). While this conclusion seems plausible owing the measurements of the long-term excess pore-pressure dissipation in the Mont Terri Rock Laboratory (Masset 2006), the rapid increase in damage of unsupported openings was unexpected and fairly new.

### 5.1.3 Apparent cohesion around tunnel excavations

Similar to a bore core and a borehole, also the rock mass in the vicinity of an underground excavation experiences unloading. Test galleries constructed in Opalinus Clay at the Mont Terri Rock Laboratory have been used to characterize the hydro-mechanical coupled behaviour of Opalinus Clay during tunnel excavation (Martin et al. 2004; Corkum and Martin 2007; Popp et al. 2008; Vietor et al. 2010; Giger et al. 2015). The short-term pore-pressure response monitored during the construction of these test galleries revealed a pore-pressure rise ahead of the tunnel face followed by subsequent reduction of pore-pressure immediately around the tunnel or slightly ahead of the tunnel face. With increasing distance from the tunnel, pore-pressure appears unaffected by construction work in the short term (Corkum and Martin 2007; Vietor et al. 2010; Amann et al. 2011; Wild et al. 2015b; Giger et al. 2015). Close to the tunnel, the pore-pressure was substantially below the in situ pore-pressure. For the majority of pore-pressure measurements conducted during the excavation of tunnels at the Mont Terri Rock Laboratory, the minimum measured pore-pressure was 100 kPa, suggesting that a conductive excavation damaged zone formed, connecting

the monitoring interval with the tunnel. The pore-pressure measurements we performed in the framework of the EZ-B experiment (Fig. 19) showed a similar behaviour at sensor BEZ-B7, where the pore-pressure rose during excavation and fell quickly in two steps to a pressure close to the atmospheric pressure as the face passed the monitoring location. In contrast, sensors BEZ-B4 and BEZ-B5 recorded pore-pressure of 40–50 kPa below atmospheric pressure. These pore-pressure measurements demonstrated for the first time that sub-atmospheric pore-pressure could develop during the excavation of galleries in Opalinus Clay, which may provide a significant apparent cohesion, at least in the short term.

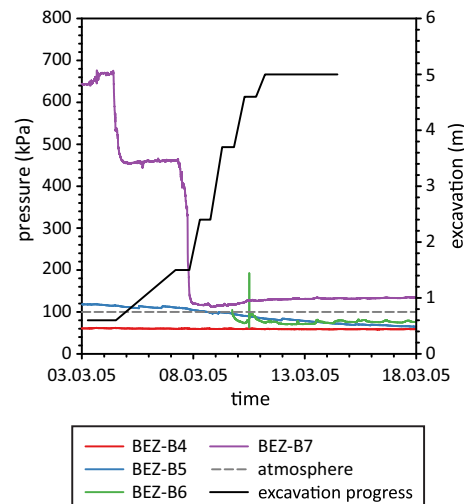


**Fig. 19** Pore-pressure response monitored around the EZB-niche during niche excavation. Modified from (Yong 2007)

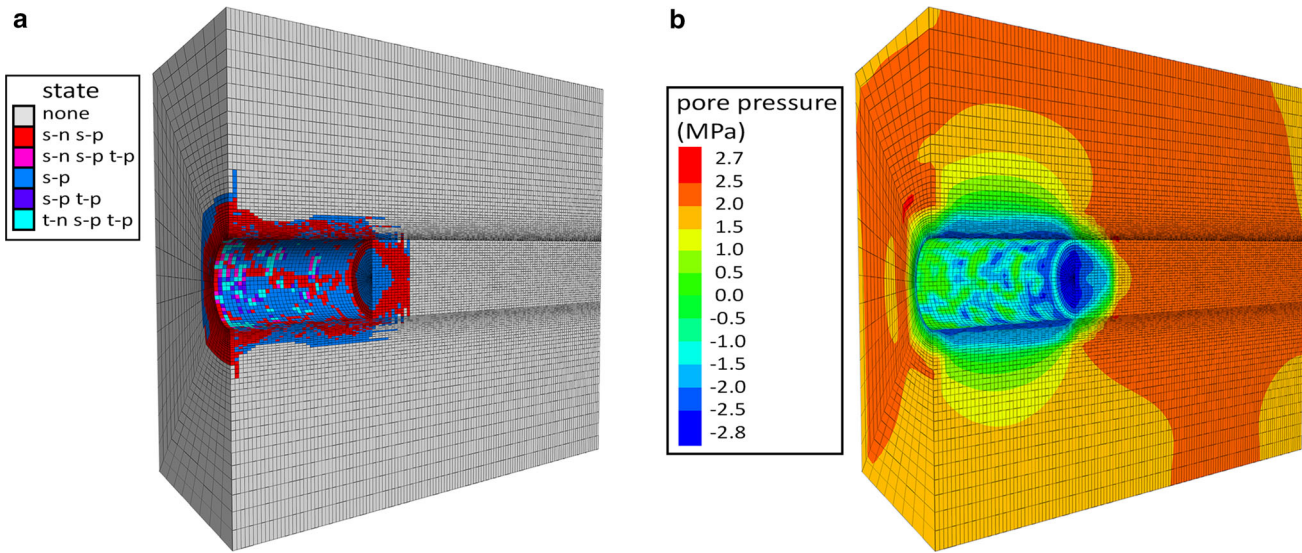


**Fig. 20** **a** Excavation damaged zone and failure mechanism (*none* elastic behaviour, no failure; *s-n* shear now, *s-p* shear past, *t-n* tension now, *t-p* tension past). **b** Short-term pore-pressure response around the excavation

We used conceptual numerical models aiming at a better understanding of the pore-pressure response in the near-field of tunnels excavated in a low permeable clay shale (Wild et al. 2015b). For the numerical analysis we used FLAC3D (Itasca 2009) and assumed an unsupported, circular opening with a diameter of 4 m that is step-wise excavated. We utilized an isotropic stress state and a stress state with  $K_0 = 0.5$  (where  $K_0$  is the ratio between the horizontal and vertical stress), and an initial pore-pressure of 2 MPa. The principal stresses and pore-pressure that evolve as a consequence of tunnel excavation were monitored in the centre of the three-dimensional model at various radial distances from the tunnel. For the fully coupled analysis we assumed that the excavation process is undrained. For the constitutive behaviour we used (1) an elastic constitutive model that was either isotropic or transversal isotropic and (2) an isotropic elastic-brittle plastic model based on a linear Mohr–Coulomb failure criterion. For further details of the numerical model see Wild et al. (2015b). The model results suggested that the pore-pressure response typically observed at the Mont Terri Rock Laboratory is a consequence of (1) the anisotropic in situ state of stress, (2) the transversal isotropic stiffness of Opalinus Clay, (3) the anisotropy ratio, (4) the orientation of the tunnel axis relative to the in situ stress state, and (5) dilatancy accompanying failure. An important outcome of this numerical study was that pore-pressure changes associated with tunnel excavation can lead to absolute negative pore-pressure of up to  $-3$  MPa in the short term (Wild et al. 2015b). In case of a transversal isotropic model, zones around the excavation with absolute negative pore-pressure are limited and the limitation depends on the assumption of the in situ stress state and the orientation of

the plane of anisotropy. In case of an elasto-plastic model, where an EDZ may develop ahead and around the advancing tunnel face (Fig. 20a), negative pore-pressure are to be anticipated within the EDZ (Fig. 20b). These negative pore-pressure are primarily related to the dilatancy that accompanies failure. The pore-pressure drop to sub-zero pore-pressure around the excavation contributes to the stability of the excavation. In the longer term, however, these negative excess pore-pressure dissipate and cause time dependent tunnel convergences. Note, however, that the rock mass close to the excavation might also dry as a consequence of the tunnel environment. This may cause an unsaturated zone with an apparent strength and stiffness significantly larger than the saturated rock, which can contribute to the stability of the excavation (Martin et al. 2004). Seasonal cyclic variations in RH may, however, cause a strength degradation and additional deformations (Walter 2015).

## 5.2 The influence of rock and rock mass anisotropy and heterogeneities on the EDZ development

Our in situ experiments showed that many fractures that form around underground excavations in Opalinus Clay are either directly or indirectly associated with bedding plane shearing or dislocations along pre-existing tectonic structures. These secondary fractures are either extensional type fractures such as horsetail splays or wing cracks or secondary shear fractures. Only when bedding plane shearing or shearing along tectonic structures was kinematically constrained, extensional type fractures initiated as primary fractures.

For a circular opening excavated parallel to the bedding plane strike (i.e. as anticipated for a repository in northern Switzerland and investigated in our study of the BDZ evolution) the behavior was dominated by bedding plane shearing and opening, and all observed extensional type fractures were secondary fractures (i.e. associated with shearing along bedding or buckling of slabs). Buckling of slabs into the unsupported boreholes developed in relatively short time and eventually borehole collapse occurred. Assuming that the behaviour observed for boreholes is representative for a mechanically excavated circular tunnel parallel to bedding, early installed rock support such as dense rock bolts covering the anticipated buckling zone, and/or shotcrete can largely prevent rock buckling and mitigate the development of large open fractures and overbreaks.

For excavations oriented normal to the bedding plane strike direction primary extensional type fractures were occasionally observed at the flat tunnel invert and at the sidewalls, were large spalls formed. Our research consistently showed that both bedding planes and tectonic fault planes dominate the formation of an EDZ.

Another important aspect that is associated with the presence of heterogeneities (i.e. tectonic fault planes, fault zones and related stiffness and strength contrasts) is the strong influence on stress redistribution around the excavation. Our numerical models demonstrate that even the presence of single tectonic fault planes substantially modify the redistributed stresses and the zone around an excavation where new fractures may evolve. Fault zones further modify the stress redistribution in both the radial and longitudinal tunnel directions. Due to stiffness contrasts between fault zones and the adjacent rock mass, large stress concentrations are to be anticipated on both sides of the fault zone. These stress concentrations lead to an intense fracturing and deformations of the rock in close vicinity to the fault zone. The zone of influence depends on the dimensions of the tunnel, the fault zone and the stiffness contrast between fault zone and the adjacent rock mass. In case of the RC mine-by experiment the zone of influence (i.e. the zone with significant modelled stress concentration) was approximately 2–3 m on both sides of the main fault.

## 6 Conclusions

The research conducted between 2003 and 2015 investigated the behaviour of intact and fractured Opalinus Clay. Our research comprised a series of laboratory experiments such as unconsolidated undrained shear tests, unconfined compression and indirect tensile strength tests on specimens equilibrated at various relative humidity and

consolidated undrained and drained triaxial tests on fully re-saturated specimens. Furthermore, three in situ experiments were carried out: an overcoring experiment and two mine-by experiments at the Mont Terri Rock Laboratory.

On the laboratory scale, we showed that even simple laboratory tests, such as unconsolidated undrained shear tests, are difficult to interpret and uncertainties remain in the representativeness of the test results. The observed shear strength, in particular the high undrained friction angle, and the bi-linear shape of the failure envelope resulting from the series of UU tests can be associated with a true material behaviour or a partly saturated state of the specimens. Partially saturated conditions are associated with suction. Our experimental studies showed that suction may develop rapidly after core extraction and substantially modifies the strength and the stiffness of the material.

Consolidated undrained tests performed on fully saturated specimens revealed a relatively small true cohesion and confirm the strong hydro-mechanical coupled behaviour of Opalinus Clay. This strong hydro-mechanical coupled behaviour, in particular pore-pressure changes that are associated with unloading stress path and the tendency of Opalinus Clay to dilate, may explain the stability of borecores and tunnel excavations in the short term. Porepressures develop which are below atmospheric pressure or rather absolute negative. This pore-pressure drop causes effective stress states that favour stability in the short term, but may cause longer-term deformations and a further development of the excavation damaged zone as the pore-pressure dissipates.

Our in situ experiment examined the formation and development of an EDZ that evolves around excavations which are excavated parallel or normal to the bedding plane orientation. Macroscopic fracturing is strongly influenced by the presence of bedding planes and tectonic fault planes. A transition from extensional macroscopic failure to shearing can be observed with increasing fault plane frequency in section where opening or shearing along bedding planes or tectonic fault planes is kinematically free. In sections where bedding plane shearing/shearing along tectonic fractures is kinematically constrained, primary extensional type fractures develop. In addition, heterogeneities such as single tectonic fault planes or fault zone substantially modify the stress redistribution and thus zones around the excavation where new fractures may form.

During our research program we observed behavioural aspect of Opalinus Clay that are either typical for rocks or soils. Due to the observed dependency of Opalinus Clay on the water content and therefore typical transitional character of the rock, our research suggests that the shaly facies of the Opalinus Clay at the Mont Terri Rock Laboratory can be classified as a, “soil-like” clay shale.

**Acknowledgements** Most of the funding of the projects described in this article was provided by the Swiss Federal Nuclear Safety Inspectorate (ENSI) with cost-sharing contributions from Swisstopo (Federal Office of Topography, Switzerland), BGR (Federal Institute for Geosciences and Natural Resources, Germany) and Chevron (USA). We also highly appreciate the scientific and technical contributions made by many partner organizations and scientists. Important partners of these projects have been ENSI (Martin Herfort, Meinert Rahn, Ernando Saraiva), BGR (Kristof Schuster, Torsten Tietz, Dieter Boeddener, Friedhelm Schulte, and Wilfried Stille), Swisstopo (Christophe Nussbaum, Nicolas Badertscher, Olivier Meier, David Jäggi, Claude Giarardin, and Lukas Glur), University of Alberta at Edmonton (Derek Martin), CEMI (Peter Kaiser, Andrew Corkum), Queen's University (Mark Diederichs), the Technical Universities of Torino (Marco Barla), TU Graz (Manfred Blümel), the Geodetic Metrology and Engineering Geodesy Group of ETH Zurich (Stephan Schütz, Florence Vaudan), and many colleagues and students from the Department of Earth Sciences at ETH (Corrado Fidelibus, Keith Evans, Frank Lemy, Valentin Gischig, Jonas von Rütte, Jürgen Hansmann, Freddy Xavier Yugsí Molina, Christian Haug, Sophie Gschwind, Sebastian Zimmer, Linda Wymann, Nicolas Kupferschmid, Patric Walter, Matthew Perras, Claudio Madonna, and Hansruedi Maurer). We are grateful two the two reviewers (Prof. Derek Martin and Dr. Bill Lanyon) for their valuable comments.

## References

- Amann, F., Button, E. A., Evans, K. F., Gischig, V. S., & Blümel, M. (2011). Experimental study of the brittle behavior of clay shale in short-term unconfined compression. *Rock Mechanics and Rock Engineering*, 44(4), 415–430.
- Amann, F., Kaiser, P. K., & Button, E. A. (2012a). Experimental study of the brittle behavior of clay shale in rapid triaxial compression. *Rock Mechanics and Rock Engineering*, 45(1), 21–33.
- Amann, F., Thoeny, R., & Martin, C. D. (2012b). Rock mechanical considerations associated with the construction of a nuclear waste repository in clay rock. In *Proceedings of the 46th US Rock Mechanics/Geomechanics Symposium 2012, Chicago*, American Rock Mechanics Association.
- Amann, F., Wild, K. M., & Martin, C. D. (2015). The role of capillary suction and dilatancy on the interpretation of the confined strength of clay shales. In *Proceedings of the 13th International Congress of Rock Mechanics/Shale Symposium, 2015, Montreal*, International Society for Rock Mechanics.
- Anagnostou, G. (2009). The effect of advance-drainage on the short-term behavior of squeezing rocks in tunneling. In *Proceedings of the International symposium on computational geomechanics, Juan-Les-Pins, France* (pp. 668–679).
- Aristomenas, G. V. (1992). *Time-dependent behavior of tunnels excavated in shale*. Ph.D. dissertation, Massachusetts Institute of Technology, Cambridge, Massachusetts, USA.
- Badertscher, N., Girardin, C., & Nussbaum, C. (2008). SE-H Experiment: EDZ structural analyses of resin impregnated sections from BSE-3 overcores. *Mont Terri Technical Note*, TN 2008-15. Federal Office of Topography (swisstopo), Wabern, Switzerland. [www.mont-terri.ch](http://www.mont-terri.ch).
- Bellwald, P. (1990). *A contribution to the design of tunnels in argillaceous rock*. Ph.D. dissertation, Massachusetts Institute of Technology, Cambridge, Massachusetts, USA.
- Bishop, A. W., & Eldin, G. (1950). Undrained triaxial tests on saturated sands and their significance in the general theory of shear strength. *Géotechnique*, 2(1), 13–32.
- Bobet, A., Aristomenas, G., & Einstein, H. H. (1999). Feasibility analysis for a radioactive waste repository tunnel. *Tunnelling and Underground Space Technology*, 13(4), 409–426.
- Bossart, P. (2008) Annex 4-12. In P. Bossart, & M. Thury (Eds.), *Mont Terri Rock Laboratory. Project, Programme 1996 to 2007 and Results*. Reports of the Swiss Geological Survey, No.3. Federal Office of Topography (swisstopo), Wabern, Switzerland. [www.mont-terri.ch](http://www.mont-terri.ch).
- Bossart, P., Bernier, F., Birkholzer, J., Bruggeman, C., Connolly, P., Dewonck, S., Fukaya, M., Herfort, M., Jensen, M., Matray, J.-M., Mayor, J. C., Moeri, A., Oyama, T., Schuster, K., Shigeta, N., Vietor, T., & Wieczorek, K. (2017). Mont Terri rock laboratory, 20 years of research: introduction, site characteristics and overview of experiments. *Swiss Journal of Geosciences*. doi:[10.1007/s00015-016-0236-1](https://doi.org/10.1007/s00015-016-0236-1) (this issue).
- Bossart, P., Trick, T., Meier, P. M., & Mayor, J.-C. (2004). Structural and hydrogeological characterisation of the excavation-disturbed zone in the Opalinus Clay (Mont Terri Project, Switzerland). *Applied Clay Science*, 26, 429–448.
- Corkum, A. G., & Martin, C. D. (2007). Modelling a mine-by test at the Mont Terri rock laboratory, Switzerland. *International Journal of Rock Mechanics and Mining Sciences*, 44, 846–859.
- Einstein, H. H. (2000). Tunnels in Opalinus Clayshale—A review of case histories and new developments. *Tunnelling and Underground Space Technology*, 15(1), 13–29.
- Giger, A. B., Marschall, P., Lanyon, B., & Martin, C. D. (2015). Hydro-mechanical response of Opalinus Clay during excavation works—A synopsis from the Mont Terri ROCK LABORATORY. *Geomechanics and Tunneling*, 8(5), 421–425.
- Golder, H. Q., & Skempton, A. W. (1948). The angle of shearing resistance in cohesive soils for tests at constant water content. In *Proceedings of the Second International Conference of Soil Mechanics and Foundation Engineering*, Vol. 1, (pp. 185–192).
- Islam, M. A., & Skalle, P. (2013). An experimental investigation of shale mechanical properties through drained and undrained test mechanisms. *Rock Mechanics and Rock Engineering*, 46, 1391–1413.
- ISRM. (1978). Suggested methods for determining tensile strength of rock materials. *International Journal of Rock Mechanics and Mining Sciences & Geomechanical Abstracts*, 15, 99–103.
- ISRM. (1979). Suggested methods for determining the uniaxial compressive strength and deformability of rock materials. *International Journal of Rock Mechanics and Mining Science & Geomechanical Abstracts*, 16(2), 135–140.
- Itasca (2009). Fast Langrangian Analysis of Continua in 3 dimensions, Version 4. *Itasca Consulting Group*, 438.
- Jaeggi, D., Nussbaum, C., Moeri, A., Shao, H., & Mueller, H. (2010). WS-H experiment: overcoring and structural analyses of the resin-impregnated BHG-B11 overcore under plane and UV light. *Mont Terri Technical Note*, TN 2010-32. Federal Office of Topography (swisstopo), Wabern, Switzerland. [www.mont-terri.ch](http://www.mont-terri.ch).
- Klinkenberg, M., Kaufhold, S., Dohrmann, R., & Siegesmund, S. (2009). Influence of carbonareous micofabric on the failure strength of claystones. *Engineering Geology*, 107, 42–54.
- Kupferschmied, N., Wild, K. M., Amann, F., Nussbaum, C., Jaeggi, D., & Badertscher, N. (2015). Time-dependent fracture formation around a borehole in a clay shale. *International Journal of Rock Mechanics and Mining Sciences*, 77, 105–114.
- Marschall, P., Distinguin, M., Shao, H., Bossart, P., Enachescu, C., & Trick, T. (2006). Creation and evolution of damage zones around a microtunnel in a claystone formation of the Swiss Jura Mountains. In *SPE International Symposium and Exhibition on Formation Damage Control*, Society of Petroleum Engineers.
- Marschall, P., Horseman, S., & Gimmi, T. (2005). Characterisation of gas transport properties of the Opalinus Clay, a potential host rock formation for radioactive waste disposal. *Oil & Gas Science and Technology*, 60(1), 121–139.

- Martin, C. D. (1997). Seventeenth Canadian Geotechnical Colloquium: The effects of cohesion loss and stress path on brittle rock strength. *Canadian Geotechnical Journal*, 34, 698–725.
- Martin, C. D., Lanyon, G. W., Bossart, P., & Blümling, P. (2004). Excavation disturbed zone (EDZ) in clay shale: Mont Terri. *Mont Terri Technical Report*, TR 01-01. Federal Office of Topography (swisstopo), Wabern, Switzerland. [www.mont-terri.ch](http://www.mont-terri.ch).
- Martin, C. D., Macchiotta, R., Elwood, D., Lan, H., & Vietor T. (2011). Evaluation of the Mont Terri Mine-By response: Interpretation of results and observations. Report to Nagra (unpublished).
- Masset, O. (2006). Rock Laboratory pore pressure long term evolution. *Mont Terri Technical Note*, TN 2006-43. Federal Office of Topography (swisstopo), Wabern, Switzerland. [www.mont-terri.ch](http://www.mont-terri.ch).
- Mazurek, M. (1998). Mineralogical composition of Opalinus Clay at Mont Terri—A laboratory intercomparison. *Mont Terri Technical Note*, TN 98-41. Federal Office of Topography (swisstopo), Wabern, Switzerland. [www.mont-terri.ch](http://www.mont-terri.ch).
- Mazurek, M., Hurford, A. J., & Leu, W. (2006). Unravelling the multi-stage burial history of the Swiss Molasse Basin: integration of apatite fission track, vitrinite reflectance and biomarker isomerisation analysis. *Basin Research*, 18, 27–50.
- Nagra (2002). Projekt Opalinuston. Synthese der geowissenschaftlichen Untersuchungsergebnisse. *Nagra Technischer Bericht*, 20-03. Nagra, Wettingen, Switzerland. [www.nagra.ch](http://www.nagra.ch).
- Neerdael, B., DeBruyn, D., Mair, R. J., & Taylor, R. N. (1999). Geotechnical behavior of Boom Clay. Commission of the European Communities. *Nuclear Science and Technology, Pilot tests on radioactive waste disposal in underground facilities*, EUR 13985, 223–238.
- Nussbaum, C., Bossart, P., Amann, F., & Aubourg, C. (2011). Analysis of tectonic structures and excavation induced fractures in Opalinus Clay, Mont Terri underground Rock Laboratory (Switzerland). *Swiss Journal of Geoscience*, 104(2), 187–210.
- Nussbaum, C., Kloppenburg, A., Caér, T., & Bossart, P. (2017). Tectonic evolution around the Mont Terri rock laboratory, northwestern Swiss Jura: constraints from kinematic forward modelling. *Swiss Journal of Geosciences*, 110. doi:[10.1007/s00015-016-0248-x](https://doi.org/10.1007/s00015-016-0248-x) (this issue).
- Pei, J. (2003). *Effect of sample disturbance in Opalinus Clay shales*. Ph.D. dissertation, Massachusetts Institute of Technology, Cambridge, Massachusetts, USA.
- Peron, H., Hueckel, T., Laloui, L., & Hu, L. B. (2009). Fundamentals of desiccation cracking of fine-grained soils: experimental characterization and mechanisms identification. *Canadian Geotechnical Journal*, 46, 7–1201.
- Popp, T., Salzer, K., & Minkley, W. (2008). Influence of bedding planes to EDZ-evolution and the coupled HM properties of Opalinus Clay. *Physics and Chemistry of the Earth*, 33, 374–387.
- Rummel, F., & Weber, U. (2004). RA experiment: rock mechanical testing and characterization on drillcores of boreholes BRA-1 and BRA-2. *Mont Terri Technical Note*, TN 2004-38. Federal Office of Topography (swisstopo), Wabern, Switzerland. [www.mont-terri.ch](http://www.mont-terri.ch).
- Schmertmann, J. H., & Osterberg, J. O. (1960). An experimental study of the development of cohesion and friction with axial strain in saturated cohesive soils. In *Research Conference on Shear Strength of Cohesive Soils* (pp. 643–694). American Society of Civil Engineers.
- Schnier, H., & Stührenberg, D. (2007). LT experiment: strength tests on cylindrical specimens, documentation and evaluation (Phases 8 & 9). *Mont Terri Technical Report*, TR 03-04. Federal Office of Topography (swisstopo), Wabern, Switzerland. [www.mont-terri.ch](http://www.mont-terri.ch).
- Skempton, A. W. (1954). The pore-pressure coefficients A and B. *Géotechnique*, 4(4), 143–147.
- Thoeny, R. (2014). *Geomechanical analysis of excavation-induced rock mass behavior of faulted Opalinus Clay at the Mont Terri Underground Rock Laboratory (Switzerland)*. Ph.D. dissertation, Swiss Federal Institute of Technology, Zürich, Switzerland.
- Thury, M., & Bossart P. (1999). Mont Terri rock laboratory, results of the hydrogeological, geochemical and geotechnical experiments performed in 1996 and 1997. *Landeshydrologie und -geologie, Geologischer Bericht No. 23*. Federal Office of Topography (swisstopo), Wabern, Switzerland. [www.mont-terri.ch](http://www.mont-terri.ch).
- Van Loon, L. R., Soler, J. M., Müller, W., & Bradbury, M. H. (2004). Anisotropic diffusion in layered argillaceous rocks: a case study with Opalinus Clay. *Environmental Science and Technology*, 38, 5721–5728.
- Vietor, T., Armand, G., Nyonoya, S., Schuster, K., & Wieczorek, K. (2010). Excavation induced damage evolution during a mine-by experiment in Opalinus clay. In *Proceedings of the 4th Int. Meeting on Clays in Natural & Engineered Barriers for Nuclear Waste Confinement*, Nantes, France.
- Walter, P. (2015). *Environmental degradation of Opalinus Clay with cyclic variations in relative humidity*. Master thesis, Swiss Federal Institute of Technology, Zürich, Switzerland.
- Wild, K. M., Amann, F., & Martin, C. D. (2015a). Dilatancy of clay shales and its impact on pore pressure evolution and effective stress for different triaxial stress paths. In *Proceedings of the 49th US Rock Mechanics/Geomechanics Symposium*, American Rock Mechanics Association.
- Wild, K. M., Amann, F., & Martin, C. D. (2015b). Some fundamental hydromechanical processes relevant for understanding the pore pressure response around excavations in low permeable clay rocks. In *Proceedings of the 13th International Congress of Rock Mechanics*. International Society for Rock Mechanics.
- Wild, K. M., Wymann, L. P., Zimmer, S., Thoeny, R., & Amann, F. (2015c). Water retention characteristics and state-dependent mechanical and petro-physical properties of a clay shale. *Rock Mechanics and Rock Engineering*, 48, 427–439.
- Yong, S. (2007). *A three-dimensional analysis of excavation-induced perturbations in the Opalinus Clay at the Mont Terri Rock Laboratory*. Ph.D. dissertation, Swiss Federal Institute of Technology, Zürich, Switzerland.
- Yong, S., Kaiser, P. K., & Loew, S. (2010). Influence of tectonic shears on tunnel-induced fracturing. *International Journal of Rock Mechanics and Mining Sciences*, 47, 894–907.
- Yong, S., Kaiser, P. K., & Loew, S. (2013). Rock mass response ahead of an advancing face in faulted shale. *International Journal of Rock Mechanics and Mining Sciences*, 60, 301–311.